GL-TR-90-0372

AN APPROXIMATE ANALYTICAL MODEL OF SHOCK WAVES FROM UNDERGROUND NUCLEAR EXPLOSIONS

F. K. Lamb
B. W. Callen
J. D. Sullivan

University of Illinois at Urbana-Champaign
Department of Physics
1110 West Green Street
Urbana, Illinois 61801

DTIC
ELECTE
MAY 20 1992
S D

December 1990

Scientific Report No. 1

GEOPHYSICS LABORATORY
AIR FORCE SYSTEMS COMMAND
UNITED STATES AIR FORCE
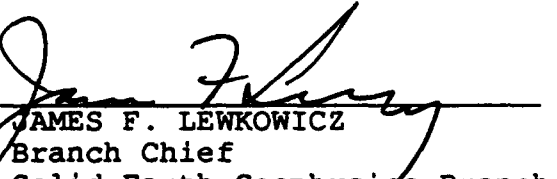HANSCOM AIR FORCE BASE, MASSACHUSETTS 01731-5000

92-13358

92 5 19 028

This technical report has been reviewed and is approved for publication.

JAMES F. LEWKOWICZ
Contract Manager
Solid Earth Geophysics Branch
Earth Sciences Division

JAMES F. LEWKOWICZ
Branch Chief
Solid Earth Geophysics Branch
Earth Sciences Division

DONALD H. ECKHARDT, Director
Earth Sciences Division

REPORT DOCUMENTATION PAGE

1 AGENCY USE ONLY (leave blank)	2. REPORT DATE	3. REPORT TYPE AND DATES COVERED
	December 1990	Scientific Report #1

4. TITLE AND SUBTITLE

An Approximate Analytical Model of Shock Waves from Underground Nuclear Explosions

5. FUNDING NUMBERS

Contract
F19628-88-K-0040
PE 62714E
PR 8A10
TA DA
WU AL

6. AUTHOR(S)

F. K. Lamb
B. W. Callen
J. D. Sullivan

7. PERFORMING ORGANIZATION NAME(S) AND ADDRESS(ES)

University of Illinois at Urbana-Champaign
Department of Physics
1110 West Green Street
Urbana, IL 61801

8. PERFORMING ORGANIZATION REPORT NUMBER

P/91/4/46

9 SPONSORING/MONITORING AGENCY NAME(S) AND ADDRESS(ES)

Geophysics Laboratory
Hanscom AFB, MA 01731-5000

Contract Manager: James Lewkowicz/LWH

10. SPONSORING/MONITORING AGENCY REPORT NUMBER

GL-TR-90-0372

11. SUPPLEMENTARY NOTES

12a DISTRIBUTION AVAILABILITY STATEMENT

12b. DISTRIBUTION CODE

13. ABSTRACT (Maximum 200 words)

We discuss an approximate analytical model for the hydrodynamic evolution of the shock front produced by an explosion in a homogeneous medium. The model assumes a particular relation between the energy of the explosion, the density of the medium into which the shock wave is expanding, and the particle speed immediately behind the shock front. The assumed relation is exact at early times, when the shock wave is strong and self-similar. Comparison with numerical simulations shows that the relation remains approximately valid even at later times, when the shock wave is neither strong nor self-similar. The model allows one to investigate how the evolution of the shock wave is influenced by the properties of the ambient medium. The shock front radius vs. time curves predicted by the model agree well with numerical simulations of explosions in quartz and wet tuff and with data from four underground nuclear tests conducted in granite, basalt, and wet tuff when the official yields are assumed. Fits of the model to data from the hydrodynamic phase of these tests give yields that are within 8% of the official yields.

14. SUBJECT TERMS

Threshold Test Ban Treaty, hydrodynamic methods, shock waves, underground nuclear explosions

15 NUMBER OF PAGES

74

16. PRICE CODE

17. SECURITY CLASSIFICATION OF REPORT	18 SECURITY CLASSIFICATION OF THIS PAGE	19 SECURITY CLASSIFICATION OF ABSTRACT	20. LIMITATION OF ABSTRACT
Unclassified	Unclassified	Unclassified	SAR

Contents

1. INTRODUCTION

Shock wave methods have long been used to estimate the yields of nuclear explosions, both in the atmosphere (see, for example, *Sedov* [1946]; *Taylor* [1950b]) and underground (see, for example, *Johnson, Higgins, and Violet* [1959]; *Nuckolls* [1959]). All such methods are based on the fact that the strength of the shock wave produced by an explosion increases with the yield, all other things being equal. As a result, the peak pressure, peak density, and shock speed at a given radius all increase monotonically with the yield. Hence, by comparing measurements of these quantities with the values predicted by a model of the evolution of the shock wave in the relevant ambient medium, the explosive yield can be estimated. Shock wave methods for determining the yields of underground nuclear explosions are of increasing interest as one means of monitoring limitations on underground nuclear testing. These methods were first introduced as a treaty-monitoring tool in the original Protocol of the Peaceful Nuclear Explosions Treaty of 1976 [*U. S. Arms Control and Disarmament Agency*, 1990a]. Hydrodynamic methods were explored further in a joint U.S.-U.S.S.R. verification experiment [*U. S. Department of State*, 1988] and have now been incorporated in new protocols to the Threshold Test Ban and Peaceful Nuclear Explosions Treaties [*U. S. Arms Control and Disarmament Agency*, 1990b].

Most shock wave algorithms for estimating the yields of underground nuclear explosions have focused on the so-called *hydrodynamic phase* (see *Lamb* [1988]), because the evolution of the shock wave during this phase is relatively simple. The energy released by a nuclear explosion initially emerges from the nuclear device as nuclear radiation, fission fragments, and thermal electromagnetic radiation (see *Glasstone and Dolan* [1977], pp. 12–25 and 61–63). At the very earliest times, energy is carried outward by the expanding weapon debris and radiation. As this debris and radiation interact with the surrounding medium, a strong shock wave forms and begins to expand. The evolution of the explosion during this phase can be followed using the equations of hydrodynamics and radiation transport. However, within ∼10–100 µs, depending on the yield and the composition and distribution of matter surrounding the nuclear charge, the outward flow of energy via radiation becomes unimportant and the explosion can be described using the equations of hydrodynamics alone. At this point the explosion enters the (purely) hydrodynamic phase. The radial stress produced by the shock wave at the beginning of this phase greatly exceeds the critical stress at which the surrounding rock becomes plastic, so that to a good approximation the shocked medium can be treated as a fluid. As the shock wave expands, it weakens. Eventually, the strength of the rock can no longer be neglected, the fluid approximation fails, and the hydrodynamic phase ends. Yield estimation methods that use measurements made during the hydrodynamic phase are called *hydrodynamic methods*.

All hydrodynamic methods require a model of the evolution of the shock wave. Models in recent or current use range in sophistication from an empirical power-law formula that supposes the evolution is completely independent of the medium (*Bass and Larsen* [1977]; see also *Heusinkveld* [1982]; *Lamb* [1988]) to multi-dimensional numerical simulations based on detailed equations of state (for recent examples of one-dimensional simulations, see *Moss* [1988]; *King et al.* [1989]; *Moran and Goldwire* [1990]). When detailed equation of state data are available, state-of-the-art numerical simulations are expected to be highly accurate, at least for spherically-symmetric, tamped explosions in homogeneous media. Nevertheless, a simple analytical model of the shock wave produced by such explosions that allows one to determine how the evolution depends on the Hugoniot and the yield is useful for several reasons. First, detailed equations of state are available only for a few geologic media. Second, large codes can be run for only a limited number of cases. Third and most importantly, an analytical model is more convenient than numerical simulations for analyzing how the evolution is affected by the properties of the ambient medium.

This is the first of several papers in which we investigate the evolution of the shock wave produced by a spherically-symmetric explosion in a homogeneous medium during the hydrodynamic phase. Such a shock wave is necessarily spherically symmetric. Here we investigate a simple analytical model. In this model, the compression of the medium at the shock front is treated exactly, using the Rankine-Hugoniot jump conditions and the Hugoniot of the ambient medium. The rarefaction of the shocked fluid that occurs as the shock front advances is treated approximately, via an *ansatz* relating the specific kinetic energy of the fluid just behind the shock front to the mean specific energy within the shocked volume. This model was proposed by *Lamb* [1987], who showed that it is exact for strong, self-similar shock waves. *Lamb* [1987] also made a preliminary comparison of the shock front radius vs. time curves predicted by the model with data from several underground nuclear explosions and numerical simulations. The model was proposed independently by *Moss* [1988], who compared its predictions with particle speed data from underground nuclear explosions and numerical simulations. Their results showed that the model provides a useful approximate description of the shock wave evolution throughout the hydrodynamic phase. The model is similar in spirit to one proposed earlier by *Heusinkveld* [1979, 1982], but is more satisfactory theoretically and appears to provide a more accurate description of underground nuclear explosions, as shown in an appendix.

In § 2 we first discuss the assumptions on which the model is based, including the *ansatz* relating the specific kinetic energy of the fluid just behind the shock front to the mean specific energy within the shocked volume. Next, we combine the *ansatz* with the Hugoniot of the ambient medium expressed as a relation between the shock speed D and the post-shock particle speed u_1 to obtain a first-order ordinary differential equation that describes the motion of the shock front. We show that solutions of this equation of motion

2

can be expressed in terms of simple analytical functions when the D vs. u_1 relation is piecewise-linear. Since an arbitrary D vs. u_1 relation can be represented to any desired accuracy by an appropriate piecewise-linear relation, the radius vs. time predictions of the model for an arbitrary Hugoniot can always be expressed as a sum of simple analytical functions. Alternatively, the equation of motion can be integrated numerically to find the model predictions for any prescribed Hugoniot. In practice, the latter approach is often more convenient. The model also gives the shock speed, post-shock density, post-shock particle speed, and post-shock pressure as functions of the shock front radius or the elapsed time, the yield of the explosion, and the Hugoniot of the ambient medium.

In § 3 we assess the accuracy of the model. We first show that the *ansatz* is exact for a shock wave that is strong and self-similar. We then compare this *ansatz* with results from numerical simulations, and find that it is also remarkably accurate for spherical shock waves that are neither strong nor self-similar. Finally, we compare the radius vs. time and particle velocity vs. radius curves predicted by the model with the corresponding curves obtained from numerical simulations of underground nuclear explosions. We conclude that the model with point-source boundary conditions provides a remarkably good description of the spherically-symmetric shock waves produced by such explosions.

In § 4 we show that the radius vs. time curves given by the analytical model of § 2 provide an excellent description of the field data from four underground nuclear tests conducted by the United States, despite the fact that these tests are not point explosions and that the ambient media may be nonuniform. In fact, the model sometimes describes the data accurately even well beyond the hydrodynamic phase of the explosion. When the model and the Hugoniots of § 3 and § 4 are used to estimate yields using data from the hydrodynamic phase of these four nuclear explosions, the resulting estimates are within 8% of the official yields. For comparison, when the numerical simulations described in § 3 are fitted to the same data, the resulting yield estimates are within 9% of the official yields. Our lack of knowledge of the geometry of these tests, of the way in which the data was gathered, and, in the case of one explosion, of the medium in which the explosion occurred, make it difficult to assess whether the relatively small differences between the various yield estimates are due to errors in the radius vs. time data, departures from spherical symmetry due to asphericity of the source and/or inhomogeneity of the ambient medium, uncertainties in the yield standard, or inadequacies of the models. The *U. S. Department of State* [1986a,b] has claimed that hydrodynamic methods are accurate to within 15% (at the 95% confidence level) of radiochemical yield estimates for tests with yields greater than 50 kt in the geologic media found at the Nevada Test Site (see also *U. S. Congress, Office of Technology Assessment* [1988]; *Lamb* [1988]). Thus, the analytical model of § 2 appears to be competitive with other models for purposes of yield estimation. A preliminary account of this work has been given by *Callen et al.* [1990b].

2. MODEL

In this section, we first present the fundamental assumptions of the model and derive the resulting equation of motion for the shock front. We then solve this equation of motion and discuss the scalings allowed by the shock-front radius vs. time curve predicted by the model.

Assumptions

The model assumes that the shock wave is purely hydrodynamic, i.e., that transport of energy via radiation is negligible and that the stress produced by the shock wave is much larger than the critical stress at which the medium becomes plastic. The model assumes further that the medium in which the shock wave is propagating is homogeneous, and that the shock wave is spherically symmetric at the time the model first applies. The shock wave therefore remains spherically symmetric. As the shock wave expands and weakens, the strength of the ambient medium eventually becomes important. At this point the model is no longer applicable.

Part of the energy released in any nuclear explosion escapes without contributing to the energy of the shock wave (see *Glasstone and Dolan* [1977], pp. 12–13). Thus, the yield measured by hydrodynamic methods is less than the total energy released in the explosion. Here we are concerned exclusively with the hydrodynamic phase of the explosion, and hence the yield W to which we refer is the so-called *hydrodynamic yield*, namely, the energy that contributes to the formation and evolution of the shock wave. The model assumes that W is constant in time. This is expected to be an excellent approximation during the hydrodynamic phase.

The Rankine-Hugoniot jump conditions express conservation of mass, momentum, and energy across the shock front (see, for example, *Zel'dovich and Raizer* [1967, Chapter I]). The model is based on approximate forms of the jump conditions, which are nevertheless extremely accurate under the conditions of interest. The model neglects the pressure p_0 of the unshocked ambient medium in comparison with the pressure p_1 of the fluid just behind the shock front. Since p_1 is $\gtrsim 1$ GPa for the times and shock radii of interest, whereas p_0 is ~ 20 MPa, neglecting p_0 is an excellent approximation. The model also neglects the specific internal energy ε_0 of the unshocked medium in comparison with the specific internal energy ε_1 of the fluid just behind the shock front. This approximation is also highly accurate, since ε_1 is greater than ε_0 for post-shock particle speeds u_1 greater than about 100 m/s, and u_1 is $\gtrsim 1$ km/s for the times and shock front radii of interest.

With these approximations, the Rankine-Hugoniot equations, written in the frame in which the unshocked material is at rest, become

$$\rho_1(D - u_1) = \rho_0 D, \tag{1}$$

4

$$\rho_0 D u_1 = p_1 \,, \tag{2}$$

and

$$\tfrac{1}{2} p_1 \left(\frac{1}{\rho_0} - \frac{1}{\rho_1} \right) = \tfrac{1}{2} u_1^2 = \varepsilon_1 \,, \tag{3}$$

where $D = dR/dt$ is the speed of the shock front, and ρ_0 and ρ_1 are the densities just ahead of and just behind the front. Equation (3) shows that the energy $p_1(1/\rho_0 - 1/\rho_1)$ acquired by a unit mass of the medium as a result of shock compression is divided equally between kinetic energy of bulk motion and the increase in the specific internal energy. The shock speed D is related to the post-shock particle speed u_1 by the Hugoniot

$$D = D(u_1) \,, \tag{4}$$

which depends on the medium.

Without loss of generality, the specific kinetic energy of the fluid just behind the shock front can be related to the mean specific energy within the shocked volume via the expression

$$u_1^2 = f \left(\frac{3W}{4\pi R^3 \rho_0} \right) \,, \tag{5}$$

where f is a dimensionless factor that generally depends on the equation of state of the ambient medium and the radius of the shock front. *A key assumption of the model is that f is independent of the shock front radius R for all shock front radii of interest.* We assess the validity of this *ansatz* in the next section, where we show that it is exact when the shock wave is strong and is approximately valid throughout the hydrodynamic phase of the explosion.

The model treats the compression of the ambient medium at the shock front exactly, since the jump conditions and the Hugoniot are correctly incorporated. On the other hand, the rarefaction that occurs as a shocked fluid element is left behind by the advancing shock front is treated only indirectly, and approximately, via the parameter f. The value of this parameter depends on the density, velocity, and specific internal energy distributions within the shocked volume, distributions that would be determined in a full hydrodynamic calculation of the structure and evolution of the shock wave. In order to carry out such a calculation, knowledge of the equation of state off the Hugoniot (i.e., along the release adiabat) is required. This requirement is sidestepped in the model by assuming that f is independent of R. The parameter f is then the only free parameter in the model.

The best value of f to use for explosions in a given rock can be determined by fitting the post-shock particle-speed relation (5) (or the relations for the shock speed, shock front radius, and post-shock pressure that follow from it) to data from numerical simulations or data from actual underground explosions in that rock. Once f is determined, the model

5

provides a description of the properties and evolution of the shock wave produced by an explosion of any yield in the same medium.

Predicted Radius vs. Time

With the assumption that f is independent of R, the right side of equation (4) becomes a known function of R and hence equation (4) becomes a first-order ordinary differential equation for R. This equation can be integrated directly to determine the radius of the shock front as a function of time. Solutions of the shock front equation of motion can be expressed in terms of simple analytical functions when the shock speed is a linear or piecewise-linear function of the post-shock particle speed, as we now show.

Linear Hugoniots.—Experimental studies of shock waves in solids (see, for example, Zel'dovich and Raizer [1967], Chapter XI) have shown that for many materials, the relation between the speed D of a shock front and the particle speed u_1 just behind it is approximately linear for large u_1, that is

$$D(u_1) \approx A + Bu_1, \tag{6}$$

for some constants A and B. In general, the $D(u_1)$ relation deviates from this high-speed relation as the post-shock particle speed falls. If we assume for the moment that $D(u_1)$ can be adequately represented by a single linear relation of the form (6) over the full range of u_1 that is of interest, we can obtain an interesting and useful analytical solution for the motion of the shock front.

First, for convenience we introduce the dimensionless variables

$$x \equiv R/L \quad \text{and} \quad \tau \equiv t/T, \tag{7}$$

where

$$L = \left(\frac{3fWB^2}{4\pi\rho_0 A^2}\right)^{\frac{1}{3}} \quad \text{and} \quad T = \frac{L}{A}. \tag{8}$$

The characteristic length L and the characteristic time T depend on the medium through the constants ρ_0, A, B, and f, and scale as the cube root of the yield W. Making use of relation (5) and the characteristic length L, the equation (6) becomes

$$D \equiv \frac{dR}{dt} = A\left[1 + \left(\frac{L}{R}\right)^{\frac{3}{2}}\right]. \tag{9}$$

This equation shows that the length L is the radius that separates the strong shock regime, where $D \propto R^{-3/2}$, from the low-pressure plastic wave regime, where $D \approx \text{const}$. In non-dimensional form, equation (9) is

$$\frac{dx}{d\tau} = 1 + \left(\frac{1}{x}\right)^{3/2}. \tag{10}$$

6

The general solution of equation (10) is

$$\tau - \tau_0 = h(x) - h(x_0),\tag{11}$$

where $\tau_0 = t_0/T$ and $x_0 = R_0/L$. Here R_0 is the radius of the shock front at t_0, the time at which the evolution of the shock wave is first described by the model. The function $h(x)$ in equation (11) is given by

$$h(x) \equiv x + \frac{1}{3}\ln\left(\frac{x + 2\sqrt{x} + 1}{x - \sqrt{x} + 1}\right) - \frac{2}{\sqrt{3}}\left[\frac{\pi}{6} + \tan^{-1}\left(\frac{2\sqrt{x} - 1}{\sqrt{3}}\right)\right].\tag{12}$$

For a point explosion, $x_0 = 0$ at $\tau_0 = 0$. For such explosions, the function $x(x_0, \tau_0, \tau)$ defined implicitly by equation (11) becomes, at small radii ($x \ll 1$),

$$x(\tau) \approx (5/2)^{2/5}\tau^{2/5},\tag{13}$$

which is the well-known temporal behavior of a *strong, self-similar shock wave* produced by a point explosion [Sedov, 1959]. At large radii ($x \gg 1$), this function becomes

$$x(\tau) \approx \text{const.} + \tau,\tag{14}$$

which describes a constant-speed plastic wave (this is sometimes referred to as a *bulk wave*). Equation (11) thus provides an interpolation between the strong shock wave and the low-pressure plastic wave regimes.

Within the assumptions of the model, an *explosion* is completely defined by its yield W and the ambient medium, which in turn is completely defined by the quantities ρ_0, A, B, and f. The shock front radius vs. time curve for an explosion of *any* yield in *any* medium can be generated from the function $x(x_0, \tau_0, \tau)$ by using the relation

$$R(t) = L\,x\left(\frac{R_0}{L}, \frac{t_0}{T}, \frac{t}{T}\right).\tag{15}$$

For a point explosion, this simplifies to

$$R(t) = L\,x(t/T).\tag{16}$$

The radius vs. time curve (15) satisfies a scaling involving the yield W and the properties A, B, and ρ_0 of the ambient medium. In particular, relation (15) implies that if the radius vs. time curve for explosion i is known, then the radius vs. time curve for a second explosion j can be generated, provided that ρ_0, A, B, f, and W are known for both explosions and the initial radii and times R_{0i}, t_{0i}, R_{0j}, and T_{0j} satisfy

$$R_{0j} = (L_j/L_i)\,R_{0i} \qquad \text{and} \qquad t_{0j} = (T_j/T_i)\,T_{0i}.\tag{17}$$

7

Under these conditions, *the radius vs. time curve $R_j(t)$ for explosion j is given in terms of the curve $R_i(t)$ for explosion i by the similarity transformation*

$$R_j(t) = (L_j/L_i)\, R_i(T_i t/T_j)\,. \tag{18}$$

The required scaling (17) is satisfied trivially if both explosions are point explosions. The similarity transformation (18) can be used to shed light on the physical origin of the so-called "insensitive interval" and to develop optimal weighting schemes for radius vs. time data (*Lamb, et al.* [1991]; for preliminary accounts, see *Lamb et al.* [1989] or *Callen et al.* [1990a]).

A special case of equation (18) that we use in the next sections is the case of explosions in identical ambient media. According to equation (18), the radius vs. time curves of two such explosions satisfy

$$R_j(t) = (W_j/W_i)^{1/3}\, R_i(W_i^{1/3} t/W_j^{1/3})\,, \tag{19}$$

provided that

$$R_{0j} = (W_j/W_i)^{1/3}\, R_{0i} \quad and \quad t_{0j} = (W_j/W_i)^{1/3}\, T_{0i}\,. \tag{20}$$

In other words, the radius vs. time curves scale with the cube-root of the yield if the initial radii and times scale with the cube-root of the yield. This result illustrates the more general point that cube-root scaling does not follow from the hydrodynamic equations and the jump conditions alone; in addition, the relevant properties of the hydrodynamic source must scale [*Lamb et al.*, 1991b]. The required scaling of the source is again satisfied trivially if both explosions are point explosions. This is consistent with the known validity of cube-root scaling during the hydrodynamic phase for point explosions in uniform media (*King et al.* [1989]; *Lamb et al.* [1991b]).

So far, we have discussed the predictions of the model for the post-shock particle speed u_1 as a function of R (eq. [5]), shock speed D as a function of R (eq. [9]), and shock front radius R as a function of time (eq. [15]). The model also predicts the evolution of other quantities of interest, including the mass density, specific internal energy, and pressure immediately behind the shock front. Expressions for these quantities can be obtained from the jump conditions (1), (2), and (3) by substituting expressions (5) and (9) for u_1 and D.

The predicted post-shock mass density is

$$\rho_1 = \left(\frac{x^{3/2} + 1}{x^{3/2} + 1 - B^{-1}} \right) \rho_0\,, \tag{21}$$

8

where $x = R/L$ is the dimensionless shock front radius. For $x \ll 1$, $\rho_1 \approx [B/(B-1)]\rho_0$, which is the limiting value for a strong shock wave. For large radii, ρ_1 approaches ρ_0, as it must. The predicted post-shock specific internal energy is

$$\varepsilon_1 = \frac{A^2}{2B^2}\frac{1}{x^3},\tag{22}$$

while the predicted post-shock pressure p_1 is

$$p_1 = \frac{\rho_0 A^2}{B}\left(\frac{1}{x^{3/2}} + \frac{1}{x^3}\right).\tag{23}$$

For small radii ($x \ll 1$), $p_1 \approx \rho_0(A^2/B)\,x^{-3}$, whereas for large radii, $p_1 \approx (\rho_0 A^2/B)\,x^{-3/2}$.

Arbitrary Hugoniots.— Although for many materials the Hugoniot at high particle speeds (or equivalently, at high pressures) is well-described by a single linear relation of the form (6), the Hugoniot at lower particle speeds usually deviates from the high-speed relation. If the linear relation that is valid at high particle speeds could be extrapolated to small u_1, the constant A would correspond to the low-pressure plastic wave speed c_0. However, such an extrapolation usually is not valid. In granite, for example, A is about 3 km/s, whereas c_0 is about 4 km/s.

Even if the Hugoniot is not linear over the range of u_1 of interest, it can still be represented to any desired accuracy by a sequence of piecewise-linear segments. In this case, equation (10) still describes the motion of the shock front within each segment of the Hugoniot, but at each break in $D(u_1)$ new Hugoniot parameters A and B must be introduced. While it is possible to write the radius vs. time curve for a piecewise-linear Hugoniot with an arbitrary number of segments as a sum of standard functions, in practice it is more convenient to treat this case by integrating the shock front equation of motion (9) numerically.

In integrating equation (9), we handled the transitions between different linear segments of the Hugoniot as follows. The transitions occur at a sequence of fixed points in u_1, which, for a given yield, are related to a sequence of radii by equation (5). After each time step, we computed the new value of the particle speed from equation (5) and compared it with the particle speed u_1^i at the junction of the $(i-1)$st segment of the Hugoniot and the ith segment. When the newly computed value of u_1 dropped below u_1^i, in the next integration step we replaced the constants A_{i-1} and B_{i-1} that described the previous segment of the Hugoniot with the constants A_i and B_i that described the current segment. The transition points between the different linear segments of the Hugoniot are not readily apparent in the resulting radius vs. time curve, because steps occur only in the *second derivative* of the shock front radius with respect to time; both $R(t)$ and its first derivative are continuous.

The radius vs. time curve predicted by the model for an arbitrary Hugoniot satisfies the cube-root scaling relation (19), provided that the initial conditions satisfy equation (20).

9

3. COMPARISONS WITH ANALYTICAL MODELS
AND NUMERICAL SIMULATIONS

In this section we assess the accuracy of the model. We first derive a general expression for the dimensionless factor f, and show that the constancy of f is exact for a point explosion in a homogeneous medium when the shock wave is strong.[1] We then explore the validity of relation (5) with f constant when the shock is no longer strong, by comparing predictions of the model with numerical simulations of underground nuclear explosions in quartz and wet tuff.

Expression for f

In order to evaluate the accuracy of the *ansatz* that f is constant, we make use of the assumption that the hydrodynamic energy of the matter interior to the shock front is conserved, that is

$$W \equiv 4\pi \int_0^{R(t)} \rho(r,t) \left[\tfrac{1}{2} u^2(r,t) + \varepsilon(r,t) \right] r^2 \, dr = \text{const.} \qquad (24)$$

To turn equation (24) into a relationship between u_1 and W, we first introduce the time-dependent dimensionless radius $\xi = r/R(t)$. Then, the distributions $\rho(r,t)$, $u(r,t)$, and $\varepsilon(r,t)$ inside the shocked volume may be rewritten, *without loss of generality*, as

$$\rho(r,t) = g(\xi,t)\,\rho_1(t)\,, \quad u(r,t) = w(\xi,t)\,u_1(t)\,, \quad \text{and} \quad \varepsilon(r,t) = e(\xi,t)\,\varepsilon_1(t)\,, \qquad (25)$$

where $\rho_1(t)$, $u_1(t)$, and $\varepsilon_1(t)$ are the mass density, particle speed, and specific internal energy just behind the shock front (where $\xi = 1$). It will be convenient to express the post-shock mass density ρ_1 in terms of the pre-shock density ρ_0 via the dimensionless factor

$$\kappa(t) \equiv \rho_1/\rho_0\,. \qquad (26)$$

---

[1] A *strong* shock wave is one in which the speed of the shock front is much larger than the speed of sound in the undisturbed rock, the pressure behind the shock front is predominantly thermal, and the ratio of the density immediately behind the shock front to the density ahead of the front is close to its limiting value. Such shock waves have special properties. In particular, the shock wave produced by a point explosion is self-similar while it remains strong (see *Zel'dovich and Raizer* [1967], Chapters I and XII). The condition that a shock wave be strong is *not* the same as the condition that the shock produce a radial stress greater than the critical stress at which the rock becomes plastic. The latter is the *hydrodynamic* condition, which is usually satisfied for some time after the shock wave is no longer strong (see § 4).

Using equations (25) and (26), equation (24) can be rewritten as

$$
\frac{W}{4\pi R^3 \rho_0} = \kappa(t) \int_0^1 g(\xi,t) \left[\tfrac{1}{2} u_1{}^2(t)\, w^2(\xi,t) + \varepsilon_1(t)\, e(\xi,t) \right] \xi^2 \, d\xi
$$
$$
= \tfrac{1}{2} u_1{}^2(t)\, \kappa(t) \int_0^1 g(\xi,t) \left[w^2(\xi,t) + e(\xi,t) \right] \xi^2 \, d\xi \,,
$$
(27)

where in the last line we have used equation (3). Comparison of equation (27) with the *ansatz* (5) gives a useful expression for the dimensionless factor f, namely,

$$
\frac{1}{f(t)} = \tfrac{3}{2}\, \kappa(t) \int_0^1 g(\xi,t) \left[w^2(\xi,t) + e(\xi,t) \right] \xi^2 \, d\xi \,.
$$
(28)

Equation (28) is merely a re-expression of equation (24) and therefore is completely general. It shows that $f(t)$ depends on the density, velocity, and specific internal energy distributions within the shocked volume at time t. We now investigate the value of $f(t)$ and its variation with time.

Strong shock interval.—Consider for simplicity a point explosion during the interval when the shock wave is strong. As noted above, during this interval the ratio of the density ρ_1 behind the shock front to the density ρ_0 ahead of the shock front approaches a limiting value (see Zel'dovich and Raizer [1967], p. 708). Thus, κ is independent of time and independent of W in this interval. Moreover, during the strong shock interval the shock wave produced by a point explosion is self-similar. Therefore, the profiles g, w, and e are also independent of time and independent of W. Thus, f is independent of time and independent of W in the strong shock interval.

For a medium that is adequately described by a Mie-Grüneisen equation of state with a constant Grüneisen coefficient, the value of f in the strong shock interval can be calculated by comparison with the solution for a self-similar shock wave produced by a strong point explosion [Sedov, 1946, 1959; Taylor, 1950a] as follows.

The Mie-Grüneisen equation of state assumes that the total pressure p is the sum of two parts: a thermal pressure p_T, which depends on the temperature and density, and a cold pressure p_c, which depends only on the density, that is,

$$
p = p_T(\rho, T) + p_c(\rho) = \rho \Gamma \varepsilon_T + p_c(\rho) \,,
$$
(29)

where ε_T is the thermal component of the internal energy and Γ is the Grüneisen coefficient (see, for example, Zel'dovich and Raizer [1967], p. 697). The thermal pressure p_T increases with the strength of the shock, whereas the cold pressure p_c is bounded, since ρ approaches a limiting value. Thus, in the strong shock interval the cold pressure term in equation (29) can be neglected (see Zel'dovich and Raizer [1967], pp. 708–709). If in addition the

Grüneisen coefficient is constant, this equation of state has the form considered by *Sedov* and *Taylor* in their solution.

The dependence of f on Γ in the strong shock interval can be calculated from equation (28) using *Sedov's* solution for the functions κ, $g(\xi)$, $w(\xi)$, and $e(\xi)$ (see, for example, *Landau and Lifshitz* [1987], pp. 403–406, for explicit expressions for κ, g, w, and e). The result is shown in Figure 1. When the shock wave is no longer strong, or when it never was strong, a value of f different from that given by Figure 1 may give a more accurate description of the shock wave evolution.

Actual nuclear tests are not point explosions but are generated by aspherical sources of finite size. In part to give the shock wave time to become more spherically symmetric, radius vs. time measurements are usually made at scaled radii ~ 2–5 m/kt$^{1/3}$ for tests with yields ~ 150 kt (at larger radii, the hydrodynamic approximation is no longer valid). At these radii, the strong-shock expression for f shown in Figure 1 is no longer accurate. As we now show, $f \approx 0.53$ appears to give a relatively accurate description of the evolution of shock waves in granite and wet tuff during the interval in radius where measurements are usually made.

Assessment of Particle-Speed Predictions

The behavior of f when the shock wave is not strong can be investigated by comparing the predictions of the *ansatz* (5) with shock wave data from actual and simulated nuclear explosions.

Lamb [1987] showed that the radius vs. time curves predicted by equations (4) and (5) agree fairly well with radius vs. time data from a numerical simulation of a nuclear explosion in wet tuff by the P-15 (CORRTEX) Group at Los Alamos National Laboratory and with field data from the *Piledriver* and *Cannikin* nuclear tests, which were conducted in granite and basalt, respectively. A more detailed comparison of the radius vs. time curves predicted by the model with data from numerical simulations is presented at the end of this section. The predictions of the model are compared with field data from underground nuclear tests in § 4.

A more direct test of the *ansatz* (5) can be made by comparing the post-shock particle speed it predicts with post-shock particle speed data from nuclear tests and numerical simulations. *Perret and Bass* [1975] have summarized a large collection of particle speed data obtained from underground nuclear explosions. *Moss* [1988] has shown that these data agree fairly well with the scaling $u_1 \propto R^{-3/2}$ predicted by relation (5), for particle speeds $\gtrsim 1$ km/s. These data appear roughly consistent with this scaling even for particle speeds as low as $\sim 10^{-4}$ km/s. *Moss* [1988] also compared the *ansatz* (5) with post-shock particle speeds from his numerical simulations of 125 kt nuclear explosions in quartz and wet tuff. He found that for particle speeds between 1 and 30 km/s, both the radius and the

density dependence of his granite and wet tuff data are accurately described by relation (5) with $f = 0.53$.

To assess the *ansatz* (5) further, we compare it with post-shock particle speed data obtained from simulations of 100 kt nuclear explosions in quartz and wet tuff. These simulations were performed by the Los Alamos CORRTEX group using the radiation hydrocode described by *Cox et al.* [1966]. In order to compare equation (5) with the simulations, we have had to reconstruct the post-shock particle speeds using appropriate Hugoniots and the radius vs. time curves obtained from the simulations. The radius vs. time curves were kindly provided to us by D. Eilers (private communication, 1987).

The reconstruction process can distort the particle speed curve if the Hugoniot used in the reconstruction differs from the Hugoniot used in the simulation. Throughout this paper, when modeling shock waves in quartz we use the Hugoniot data compiled by *King et al.* [1989] from several sources [*Chung and Simmons,* 1969; *Al'tshuler et al.,* 1977; *Wackerle,* 1962; *McQueen et al.,* 1977; *Ragan,* 1984]. These data are shown in Figure 2. An expanded view of the low-u_1 section of the data is shown in Figure 3. When comparing with the quartz simulations of the Los Alamos CORRTEX group, we use a piecewise-linear representation of the data compiled by *King et al.,* using their interpolation at low post-shock particle speeds (indicated by the dash-dotted line in Figure 3). In modeling shock waves in wet tuff, we use the piecewise-linear Hugoniot given by *King et al.* [1989], which is shown in Figure 4. The light solid curves in Figures 3 and 4 show where the post-shock pressure calculated from the jump condition (2) is 15 GPa. For the reasons discussed in § 4, we adopt this pressure as marking the end of the hydrodynamic phase. We believe these Hugoniots are very close to the Hugoniots used in the numerical simulations, but we cannot rule out the possibility of some distortion.

Figure 5 shows that relation (5) with $f = 0.53$ provides an excellent description of the post-shock particle speed data from the simulated explosion in quartz, for particle speeds from ~30 down to ~0.6 km/s. Figure 6 shows that relation (5) with $f = 0.53$ also provides an excellent description of the post-shock particle speed data from the simulated explosion in wet tuff, for particle speeds from ~40 down to ~1 km/s.

On the basis of these comparisons, we conclude that relation (5) with $f = 0.53$ provides a good description of the relation between the yield, the mass density of the ambient medium, the radius of the shock front, and the post-shock particle speed during the hydrodynamic phase of the explosion, including times when the shock wave is no longer strong.

Assessment of Radius vs. Time Predictions

In order to assess further the accuracy of the model, we compare the radius vs. time curves that it predicts with the corresponding curves predicted by numerical simulations

13

of underground nuclear explosions in quartz and wet tuff. We set f equal to 0.53 and use point-source boundary conditions when solving equation (10) here and throughout this paper.

Quartz.—As described above, the Los Alamos CORRTEX Group (D. Eilers et al.) has simulated a 100 kt nuclear explosion in quartz. We compared the present model with this simulation, using both a linear description of the quartz Hugoniot and the more complete piecewise-linear description discussed above. These Hugoniots are indicated respectively by the dashed and dash-dotted lines in Figures 2 and 3. The mass density used in the model was the same as that used in the simulation, namely 2650 kg/m^3.

Figure 7 compares the radii predicted by the model with the radii predicted by the simulation. The top panel shows these radii as functions of time, whereas the bottom panel displays the relative difference

$$\delta \equiv \left(\frac{R_{data}(t) - R_{model}(t)}{R_{data}(t)} \right) \tag{30}$$

between these radii. The dashed curve is the value of δ that results from using the linear description of the Hugoniot in the analytical model, whereas the dash-dotted curve is the result given by using the piecewise-linear Hugoniot. When the linear approximation to the Hugoniot is used, the absolute value of δ is less than 5% before 0.7 ms but rises to ~12% by ~5 ms. As expected from the behavior of the actual Hugoniot, the radii predicted by the linear approximation are systematically too large at late times. When the more accurate piecewise-linear Hugoniot is used, δ is never more than 1.8%.

Wet tuff.—The Los Alamos CORRTEX Group (D. Eilers et al.) has also simulated a 100 kt nuclear explosion in saturated wet tuff. We compared the present model with this simulation, again using both a linear description of the wet tuff Hugoniot and the more complete piecewise-linear description of *King et al.* [1989]. These Hugoniots are indicated respectively by the dashed and solid lines in Figure 4. The mass density used in the model was the same as that used in the simulation, namely 1950 kg/m^3.

Figure 8 compares the radii predicted by the analytical model with the radii predicted by the simulation. When the linear approximation to the Hugoniot is used, the absolute value of δ is always less than 9%. Again, as expected from the behavior of the actual Hugoniot, the radii predicted by the linear approximation are systematically too small at late times. When the more accurate piecewise-linear Hugoniot is used, the relative difference is never more than 6% and is less than 2% after 0.6 ms.

Discussion.—These comparisons of the radius vs. time curves predicted by the model with the radius vs. time curves predicted by numerical simulations confirm the earlier assessment, which was based on comparison of peak particle velocities, that the model with f set equal to 0.53 provides an excellent description of spherically-symmetric shock

14

waves from underground nuclear explosions in granite and wet tuff, during much of the hydrodynamic phase. Therefore, we shall adopt this value when comparing the model with field data from underground nuclear explosions.

4. COMPARISONS WITH FIELD DATA

In this section we use radius vs. time data from four underground nuclear tests conducted by the United States to assess the usefulness of the analytical model. The four data sets we consider are from the nuclear tests code-named *Piledriver*, *Cannikin*, and *Chiberta*, and from a test that we call *NTS-X*, since its official name remains classified. The radius vs. time data from the first three tests were obtained using the *SLIFER* technique [*Heusinkveld and Holzer*, 1964]. These data were kindly provided to us by M. *Heusinkveld* [1986; 1987, private communication]. The radius vs. time data from the test we call *NTS-X* were taken from *Heusinkveld* [1979]; the measurement technique used to obtain these data was not reported. To our knowledge, no radius vs. time measurements made using the more recently developed *CORRTEX* technique [*Virchow et al.*, 1980] are publicly available.

Any attempt to compare models or simulations of spherically-symmetric explosions in uniform media with data from underground nuclear tests must confront at the outset the fact that the shock wave produced by such a test evolves from an aspherical source of finite size into a medium that is at least somewhat inhomogeneous (see *Lamb* [1988] and *Lamb et al.* [1991c]). In comparing the predictions of the model of § 2 with data from nuclear tests, we adopt the particular solution that corresponds to a point explosion. For this solution, cube-root scaling is exact. We also assume cube-root scaling is valid when comparing the results of the numerical simulations with data from nuclear tests. Since these simulations follow the shock wave produced by an initial source of finite size, cube-root scaling is at best only approximately valid for these simulations.

In using cube-root scaling, we are tacitly assuming that the finite size of the source, the asphericity of the explosion, and any inhomogeneities in the ambient medium have a negligible effect, both in the simulations and in the actual test, by the time the shock front has expanded to the radii at which the comparison is made. Although shock waves produced by underground explosions in uniform media do tend to become more spherical with time, the properties of the source can sometimes have a significant effect during the hydrodynamic phase [*Moran and Goldwire*, 1989; *Lamb et al.*, 1991b]. Unfortunately, we are unable to assess directly the validity of our assumptions, because we lack detailed knowledge of the sources used in the numerical simulations, the conditions under which the nuclear tests were conducted, and the way in which the field data was collected.

We also lack detailed knowledge of how the official yields were determined for these four events. In using the official yields to assess hydrodynamic methods, we are implicitly assuming that they are accurate and independent of hydrodynamic methods. However, the procedure by which official yields are determined is known to be complex, and is not publicly available. It is possible in some cases that the official yields may actually be less accurate than the hydrodynamic yield estimate. Moreover, the official yield determination

16

procedure usually makes use of information derived from hydrodynamic methods, as well as radiochemical and other methods. If so, the official yield obviously is not independent of the hydrodynamic yield. Furthermore, in some cases the material properties used to obtain hydrodynamic yield estimates may have been adjusted to give better agreement with estimates obtained using other methods. The comparisons in this section show that despite the complexity of underground nuclear explosions, both the analytical model and the numerical simulations accurately describe the shock waves produced by the nuclear tests considered here, when the official yields are used.

A solution of the analytical model is determined by specifying the Hugoniot, the value of the parameter f, and the yield. The Hugoniot can in principle be determined from laboratory measurements made on samples taken from the emplacement and satellite holes. Unfortunately, if such measurements were made for the four events analyzed here, they are not publicly available. Therefore, we used generic Hugoniot data characteristic of the ambient medium of each explosion. For the reasons discussed in the preceding section, we used $f = 0.53$ throughout the present analysis.

We first assess the accuracy of the analytical model in predicting the radius of the shock front by comparing the radius vs. time curves it gives with radius vs. time data from the four nuclear tests cited above. We then investigate the usefulness of the model for yield estimation by fitting it to radius vs. time data from these tests, treating the yield as an adjustable parameter.

Radius vs. Time Curves

In comparing the radius vs. time predictions with field data, we generally used either the subset of the available data that fell within the hydrodynamic interval defined below, or, where stated, certain larger data sets. However, for *NTS-X*, we followed the recommendation of *Heusinkveld* [1979] and omitted the first nine data points from our analysis. For *Chiberta*, the first seven points were inconsistent with each other and with the remaining points, and hence these seven points were also omitted from our analysis. We now discuss the analysis of each event in turn.

Piledriver. The *Piledriver* event was an explosion conducted in granite at the Nevada Test Site on 2 June 1966 and had an announced yield of 62 kt [*U. S. Department of Energy*, 1987]. In modeling this explosion, we considered the simple linear and piecewise-linear approximations to the quartz Hugoniot shown respectively by the dashed and solid lines in Figures 2 and 3. We assumed that the granite surrounding the nuclear device had a density equal to the standard density of quartz, namely 2650 kg/m^3, and that the yield of the explosion was 62 kt. We then integrated the differential equation (10) as described in § 2.

Figure 9 compares the predictions of the analytical model with the data from *Piledriver*. The left panel shows the radius as a function of time, whereas the right panel displays the relative difference

$$\delta \equiv \left(\frac{R_{data}(t) - R_{model}(t)}{R_{data}(t)} \right) , \tag{31}$$

between the predicted and measured radii, to allow a more detailed assessment of the accuracy of the model. In both panels, the dashed curve is the result given by the simple linear approximation to the Hugoniot, whereas the solid curve is the result given by the piecewise-linear description of the full Hugoniot.

As expected, the radii given by the simple linear and the piecewise-linear Hugoniots are very similar at early times, but deviate significantly from one another at later times. When the full Hugoniot is used, the relative difference δ between the measured and predicted radii is never more than 7% and is less than 4% after 0.6 ms. When the simple linear Hugoniot is used for all particle speeds, the absolute value of δ is less than 7% before 0.6 ms but rises to ~11% after 1.2 ms. The radii predicted by the simple linear Hugoniot are systematically too large after 0.6 ms because this approximation gives shock speeds that are systematically too high when the particle speed is low (see Fig. 3). For reference, the peak pressure drops to 15 GPa at about 2.8 ms. As discussed below, we adopted this pressure as marking the end of the hydrodynamic phase.

Cannikin.—The *Cannikin* event was an explosion conducted in basalt at Amchitka Island, Alaska, on 6 November 1971. The official yield of this event remains classified; the *U. S. Department of Energy* [1987] has said only that it was less than 5 megatons. The data from *Cannikin* that were given to us had been scaled by dividing both the radius and the time measurements by the cube-root of the official yield in kilotons. If cube-root scaling were exact, this would make the radius vs. time curve appear identical to the curve that would result from detonation of a 1 kt device in the same medium. As noted above, cube-root scaling may not always be accurate for underground nuclear explosions. However, since the analytical model we are exploring exhibits exact cube-root scaling, comparisons of this model with scaled and unscaled data will give the same result. We therefore treated the data from *Cannikin* as though it had been produced by a 1 kt explosion.

To construct a Hugoniot for *Cannikin*, we used the data on Vacaville basalt obtained by *Jones et al.* [1968] and *Ahrens and Gregson* [1964]. These data and the piecewise-linear and simple linear Hugoniots that we constructed from them are shown in Figure 10. We assumed the rock surrounding the explosion had a density of 2860 kg/m^3, equal to the density of the samples measured by Jones et al.

Figure 11 compares the radii predicted by the analytical model with the radii measured during *Cannikin*. Again, the left panel shows the radius as a function of time, whereas the

right panel displays the relative difference between the predicted and measured radii. When the piecewise-linear approximation to the full Hugoniot is used, the relative difference between the radii is always less than 3%. When the simple linear Hugoniot is used for all particle speeds, the magnitude of δ is less than 5% before 0.22 ms, but increases after this time, reaching 14% at 0.6 ms, near the end of the data set. As in *Piledriver*, the radii predicted by the simple linear Hugoniot are systematically too large after 0.1 ms because this approximation gives shock speeds that are systematically too high when the particle speed is low. For reference, the peak pressure falls to 15 GPa at about 0.7 scaled ms. Thus, all the radius data from *Cannikin* lie within the hydrodynamic region.

Chiberta.— The *Chiberta* explosion was conducted in wet tuff at the Nevada Test Site on 1975 December 20. The official yield of this test remains classified; the *U. S. Department of Energy* [1987] has said only that it was between 20 and 200 kilotons. Using seismic data, *Dahlman and Israelson* [1977] estimated that the yield of *Chiberta* was 160 kt. Like the data from *Cannikin*, the radius vs. time data from *Chiberta* available to us were scaled by the cube-root of the official yield. For the reason explained above in connection with *Cannikin*, we treated the data from *Chiberta* as though it had been produced by a 1 kt explosion.

In modeling *Chiberta*, we used the linear and piecewise-linear approximations to the wet tuff Hugoniot shown respectively by the dashed and solid lines in Figure 4. We assumed that the rock surrounding the device emplacement had a density of 1950 kg/m^3.

Figure 12 compares the predictions of the analytical model with the data from *Chiberta*. Again, the dashed curve is the result given by the simple linear Hugoniot, whereas the solid curve is the result given by the piecewise-linear approximation to the full Hugoniot. As before, the radii given by the two approximations are very similar at early times, but deviate significantly from one another at late times. When the piecewise-linear Hugoniot is used, the relative difference δ between the measured and predicted radii is never more than ~4% and is $\lesssim 1\%$ between 0.35 and 1.6 ms. When the simple linear Hugoniot is used for all particle speeds, the absolute value of δ is less than 3% before 0.6 ms, but increases after this time, reaching 14% at 1.6 ms, near the end of the data set. The radii predicted by the simple linear Hugoniot are systematically too small after 0.4 ms because this approximation gives shock speeds that are systematically too low for low particle speeds (see Fig. 4). For this event, the peak pressure falls below 15 GPa at about 0.5 scaled ms. Thus, a large fraction of the radius measurements were made outside the hydrodynamic region.

NTS-X.— The event we call *NTS-X* was an explosion conducted at the Nevada Test Site. Radius vs. time data from this explosion were reported by *Heusinkveld* [1979], who stated that the official yield was 54.2 kt. Heusinkveld surmised that the ambient medium

was saturated wet tuff, the ambient medium of most tests conducted at the Nevada Test Site.

In modeling *NTS-X* we assumed that the explosion did occur in wet tuff. We followed the same procedure used in modeling *Chiberta*, except that we assumed the yield was 54.2 kt. Figure 13 compares the predictions of the analytical model with the data from *NTS-X*. As before, the radii given by the simple linear Hugoniot and by the piecewise-linear approximation to the full Hugoniot are very similar at early times, but deviate significantly from one another at later times. The relative difference δ is never more than than 5% when the piecewise-linear Hugoniot is used. When the simple linear Hugoniot is used for all particle speeds, δ is less than 5% before 2 ms, but increases after this time, reaching 17% at 6 ms, near the end of the data set. As in *Chiberta*, the radii predicted by the simple linear Hugoniot are systematically too small after 0.1 ms because this approximation gives shock speeds that are systematically too low for low particle speeds (see Fig. 4). For reference, the peak pressure falls below 15 GPa at about 2.0 ms. Like *Chiberta*, a large fraction of the radius measurements were made outside the hydrodynamic region.

Yield Estimation

Having shown that the analytical model of § 2 provides a relatively accurate description of the evolution of the shock waves produced by underground nuclear explosions for several of the geologic media found at U. S. test sites, we now consider its usefulness in yield estimation. We do this by adjusting the assumed yield to give the best fit of the model to radius vs. time data from the four U. S. nuclear tests discussed previously.

In order to determine the best fit of the analytical model to a given set of radius vs. time data, we need a measure of the goodness of the fit. This should be a function of the difference between the predicted and measured shock front radii, weighted in an appropriate way. Unfortunately, the radius data that we were furnished came without any information on the random and systematic errors. In fact, no error information is available for any of the currently declassified radius vs. time data, a large fraction of which is analyzed here.

The absence of error information made it impossible to develop a proper measure of the goodness of the fits and to determine the uncertainties of the yield estimates. We therefore adopted a very simple fitting procedure that allowed us to determine a best-fit yield and to compare fits to field data made with the analytical model and with the numerical simulations of the Los Alamos CORRTEX group. We assess the accuracy of the yield estimates made with the analytical model by comparing them with the estimates obtained by fitting numerical simulations to the same data, an approach called *simulated explosion scaling*, and by comparing them with the official yields. The precise algorithm used in

determining official yields is unknown, but presumably makes use of radiochemical and seismic as well as shock wave measurements, when these are available (see *Lamb* [1988]).

Procedure. For simplicity, we assumed that all yields are equally likely *a priori* and that the measurement errors follow a Gaussian distribution. Then the maximum of the likelihood function can be found by minimizing the properly weighted sum of the mean-square differences between the predicted and measured shock front radii (see, for example, *Mathews and Walker* [1964], § 14 7). Since we had no information on the errors of the individual measurements, we assumed that the measurements are unbiased and assigned them unit weight if they met our selection criteria (see below) or zero weight if they did not. The maximum of the likelihood function is then given by the minimum of the measure

$$\frac{1}{N} \sum_i \left(R(t_i) - R_{\text{model}}(t_i) \right)^2, \tag{32}$$

where the sum runs over the measurements used in the particular yield estimate.

The analytical model and the numerical simulations discussed in § 2 and § 3 are valid only during the hydrodynamic phase, when the strength of the ambient medium can be neglected. However, the influence of the strength of the medium increases gradually as the shock wave weakens, so there is no well-defined peak pressure at which the hydrodynamic phase ends. *Wackerle* [1962] found that in quartz, strength effects can be ignored above the critical stress, which is about 4 GPa. Studies by *Grady et al.* [1974] of quartz at pressures above 15 GPa demonstrated that strength effects are negligible in this pressure regime. Basalt becomes plastic at a critical stress of about 4 GPa [*Ahrens and Gregson*, 1964]. The critical stress for saturated wet tuff is estimated to be ~1 GPa [*Holzer*, 1965]. In the present work we have adopted the convention that the hydrodynamic phase ends in all these materials when the peak pressure falls below 15 GPa. This is a conservative criterion, in the sense the hydrodynamic phase most likely extends to lower peak pressures.

When fitting the analytical model or the simulated explosion in wet tuff of *King et al.* [1989] to field data, we determined the point at which the peak pressure fell below 15 GPa using the analytical model with the piecewise-linear representations of the full Hugoniots of § 3. When fitting the simulated explosion in SiO_2 of *King et al.* [1989] to field data, we determined the point at which the peak pressure fell below 15 GPa using the analytical model with the approximate Hugoniot adopted by *King et al.* Plots of the peak pressure predicted by the analytical model are given in the appendix.

We are interested in the accuracy of the analytical model when it is used with simple linear Hugoniots, since we use this approximation in a companion study of how the evolution of the shock wave is influenced by the properties of the ambient medium and how these properties affect the characteristic radius at which the shock wave becomes a low pressure plastic wave (*Lamb et al.* [1991a]; for a preliminary account, see *Lamb et*

al. [1989], *Callen et al.* [1990a]). We therefore compare the yields obtained by fitting the analytical model to the field data using simple linear approximations to the Hugoniots with the yields obtained using the full, piecewise-linear Hugoniots.

Although the analytical model and the numerical simulations we consider are valid only during the hydrodynamic phase, in some cases they may describe the evolution of the shock wave adequately even beyond the region where the peak stress is large compared with the critical stress of the medium. Knowing how rapidly these models become inaccurate when used outside the hydrodynamic region is important for assessing whether they can be used for yield estimation when the shock wave within the hydrodynamic region is disturbed, either because the yield is low, causing the hydrodynamic region to be close to the device canister, or because the geometry of the test is complex (see *Lamb* [1988]). In order to investigate the accuracy of the analytical model when fit to data taken at relatively large radii, we first estimated yields using only data taken during the hydrodynamic phase as defined above and then using two successively larger sets of data, defined by successively lower cutoff pressures. The radius at which the peak pressure predicted by the analytical model falls below a given pressure depends on the assumed yield. Thus, the number of data points used in evaluating expression (32) varies with the assumed yield.

Results.— The results obtained by fitting the analytical model and numerical simulations to field data from the hydrodynamic interval are summarized in Tables 1–4. The first column in each table shows which model was used: the analytical model or one of the numerical simulations discussed in § 3. The second column shows which Hugoniot was used: the simple linear approximation to the generic Hugoniot, the piecewise-linear representation of the full generic Hugoniot, the approximate SiO_2 Hugoniot of *King et al.* [1989], or the wet tuff Hugoniot of *King et al.* [1989]. The next four columns list results obtained by fitting the models with the specified Hugoniots to field data from the hydrodynamic phase. Shown are the yield estimate W_{est}, the number N of data points used in the estimate, the root-mean-square difference in radius

$$\Delta R_{rms} \equiv \left[\frac{1}{N} \sum_i \left(R(t_i) - R_{model}(t_i) \right)^2 \right]^{\frac{1}{2}} . \tag{33}$$

and the quantity $\Delta R_{rms}/W_{est}^{-1/3}$ for each fit. The last quantity can be used to compare the quality of the fits achieved for the four events. For *Piledriver* and *NTS-X*, the yield estimates are given to the nearest 0.1 kt, whereas for *Cannikin* and *Chiberta*, the estimates are given to the nearest 0.005 kt. Table 5 compares the results obtained by fitting the analytical model to data from the hydrodynamic interval with the results obtained by fitting to data sets that include data from beyond the hydrodynamic interval.

Not surprisingly, the best agreement between the official yield and the yield estimated by fitting the analytical model to the radius vs. time data is achieved when a piecewise-linear representation of the full Hugoniot is used and the model is fit only to data from the hydrodynamic phase. In this case, the difference between the official yield and the yield obtained by fitting the analytical model is 1% for *Piledriver*, 8% for *Cannikin*, and 7% for *Chiberta*. The difference between the yield quoted by *Heusinkveld* [1979] for *NTS-X* and the yield obtained by fitting the analytical model is 8%. For comparison, the differences between the official or quoted yields of these events and the yields obtained by fitting the numerical simulations to data from the hydrodynamic phase are 2%, 1%, 7%, and 1%, respectively. Thus, the yield estimates obtained by fitting the analytical model with piecewise-linear representations of the Hugoniots to data from the hydrodynamic phase are nearly as accurate as the yield estimates obtained by fitting the numerical simulations to these same data.

The agreement between the official yield and the yield estimated by fitting the analytical model with simple linear Hugoniots to data from the hydrodynamic phase is not as close, but is still remarkably good. For the events in wet tuff, the estimated yields differ from the official or quoted yields by only 0% for *NTS-X* and 5% for *Chiberta*. This is not surprising, since the simple linear approximation to the Hugoniot is nearly identical to the full, piecewise-linear representation of the Hugoniot for the particle speeds encountered during the hydrodynamic phase in the two events (see Figure 4). For the same reason, the yield of the *Cannikin* event obtained by using the analytical model with the simple linear approximation to the basalt Hugoniot differs from the official yield by only 2%. Although the relative difference $\Delta W/W$ obtained using this approximation to the Hugoniot is smaller than the relative difference obtained using the piecewise-linear representation of the full Hugoniot, the quality of the fit is somewhat poorer, as shown by the size of ΔR_{rms} (see Table 2). However, for the *Piledriver* event, the difference between the official yield and the yield obtained using the simple linear Hugoniot is ~40%, much greater than the difference when the piecewise-linear Hugoniot is used. This is not surprising, since the simple linear approximation to the SiO_2 Hugoniot is inaccurate for the particle speeds encountered during most of the hydrodynamic phase (see Figures 2 and 3).

Consider now the effect on the yield estimates when data from outside the hydrodynamic phase are included. A meaningful study of this effect is only possible for *Chiberta* and *NTS-X*, since all or almost all the available data from *Cannikin* and *Piledriver* lie within the hydrodynamic region. As shown in Table 5, the estimated yield of *NTS-X* increases from 58.5 to 66.4 and 71.5 kt when data out to peak pressures of 7.5 and 4.6 GPa are included. The differences between the latter yields and the quoted yield of 54.2 kt are 23% and 32%, respectively. For *Chiberta*, on the other hand, including data out to peak pressures of 7.5 and 4.6 GPa increases the estimated yield only slightly, from 0.930 to 0.970

23

and 0.995 kt. The differences between the latter yields and the official yield of 1.00 kt are 3% and 0.5%, respectively.

The large difference in the sensitivity of the *Chiberta* and *NTS-X* yield estimates to inclusion of data from outside the hydrodynamic interval is somewhat surprising, since both events supposedly took place in wet tuff and the data from both events extend to approximately the same scaled time ($\sim$0.6 ms/kt$^{1/3}$). However, as explained above, we do not know either the medium or the yield of *NTS-X* for certain. Furthermore, we have no knowledge of any special conditions that may have affected the explosion or the shock wave radius measurements. There does appear to be a systematic difference between the fits of the analytical model to these two events at late times. Without more information, we are unable to determine whether this difference is due to some difference in the events themselves, to systematic error in one of the sets of radius measurements, to systematic error in the Hugoniot we have used, or to inaccuracy of the analytical model when it is used so far outside the hydrodynamic region.

5. SUMMARY AND CONCLUSIONS

We have explored an approximate analytical model of the evolution, during the hydrodynamic phase, of the shock wave produced by a spherically-symmetric explosion in a homogeneous medium. The equation of motion for the shock front treats the compression of material at the front exactly, using the Rankine-Hugoniot jump conditions and the Hugoniot of the ambient medium. The rarefaction behind the shock front is treated only approximately through a parameter f that describes the distribution of the fluid variables within the shocked volume. A key assumption of the model is that f remains constant throughout the evolution of the shock wave. The model predicts the evolution of the particle speed, shock speed, mass density, pressure, and specific internal energy immediately behind the shock front, as well as the shock front radius as a function of time. For a point explosion, the model exhibits cube-root scaling, in accordance with the conservation laws for spherically symmetric point explosions in uniform media (see *King et al.* [1989] and *Lamb et al.* [1991b]).

We have shown that the parameter f, which relates the specific kinetic energy of the fluid just behind the shock front to the mean specific energy within the shocked volume, is constant when the shock wave is strong and self-similar. By comparing the relation involving f with results from numerical simulations of underground nuclear explosions in quartz and wet tuff, we have shown that it is also remarkably constant even when the shock wave is no longer strong, for explosions in these media. Furthermore, we find that the value of f is relatively independent of the ambient medium, and that $f = 0.53$ adequately reproduces the particle-speed curve extracted from the numerical simulations, in agreement with the previous results of *Moss* [1988].

The radius vs. time curves predicted by the model for a point explosion are in excellent agreement with the shock front radii measured during underground nuclear tests in granite, wet tuff, and basalt, when the official yields are assumed and f is set equal to 0.53. If the model is used with a piecewise-linear approximation to the Hugoniot, the largest differences between the predicted and measured radii range from 3% to 7% for the different events. Even when the model is used with a simple linear approximation to the Hugoniot, the shock front radii that it predicts agree extremely well with the measured radii for the events in wet tuff (*Chiberta* and *NTS-X*), where the differences are less than 3% and 6%, respectively, during the hydrodynamic phase. For the events in basalt (*Cannikin*) and granite (*Piledriver*), the high-pressure approximation works less well, but the differences in the predicted and measured radii are still less than 14% during the hydrodynamic phase. The average differences are substantially less in all cases.

We have shown that the model can also be used to estimate the yields of underground nuclear explosions, with good results. When the analytical model is used with point-source boundary conditions and a piecewise-linear representation of the Hugoniot, the

25

yields obtained by fitting the radius vs. time data from the hydrodynamic phase of the explosions are within 8% of the official yields. For comparison, the yields obtained by fitting numerical simulations carried out by the Los Alamos CORRTEX group to the same data are within 7% of the official yields. Thus, the yield estimates obtained using the analytical model are nearly as accurate as the yield estimates obtained using the numerical simulations.

More generally, the U. S. Department of State has claimed that hydrodynamic methods are accurate to within 15% (at the 95% confidence level) of radiochemical yield estimates for tests with yields greater than 50 kt in the geologic media in which tests have been conducted at the Nevada Test Site (*U. S. Department of State* [1986a,b]; see also *U. S. Congress, Office of Technology Assessment* [1988]; *Lamb* [1988]). Thus, the analytical model appears to be competitive with existing models for estimating the yields of underground nuclear tests conducted in relatively uniform media.

In a companion paper [*Lamb et al.*, 1991a], we use the analytical model studied here to investigate hydrodynamic yield estimation algorithms more fully, including optimal weighting of radius vs. time data (a preliminary account of this work has been given in *Lamb et al.* [1989] and *Callen et al.* [1990a]). In a subsequent paper [*Lamb et al.*, 1991b], we analyze the validity of cube-root scaling for spherically-symmetric underground nuclear explosions, using similarity transformation methods and numerical simulations to explore the effects of source size and composition.

APPENDIX: COMPARISON WITH HEUSINKVELD'S MODEL

In this appendix, we compare the approximate analytical model of § 2 with the approximate model proposed by *Heusinkveld* [1979, 1982]. Both models neglect the specific internal energy and pressure of the ambient medium. Both also predict radius vs. time curves that exhibit the temporal behavior characteristic of a strong, self-similar shock wave at early times, then enter a gradual transition period, and finally exhibit the temporal behavior of a low-pressure plastic wave. However, Heusinkveld's model differs from the model of § 2 in several important respects.

First, Heusinkveld assumed that the *internal energy per unit volume* just behind the shock front, namely $e_1 = \rho_1 \varepsilon_1$, is a constant fraction f_H of the *total energy per unit volume* within the shock front, that is,

$$e_1 = \frac{3 f_H W}{4 \pi R^3} .$$ (A1)

In contrast, the model of § 2 assumes that the *specific kinetic energy* of the fluid just behind the shock front is a constant fraction f of the *total specific energy* within the shock front (see eq. [5]); *the specific internal energy* just behind the shock front is equal to the specific kinetic energy there (see eq. [3]).

Second, Heusinkveld's model satisfies only the momentum jump condition (2), whereas the model of § 2 satisfies all three jump conditions (1), (2), and (3). In place of the specific internal energy jump condition (3), Heusinkveld assumed that the pressure just behind the shock front is proportional to a constant coefficient Γ times the energy per unit volume there, that is,

$$p_1 = \Gamma e_1 .$$ (A2)

As noted in § 3, this is the strong shock limit of the Mie-Grüneisen equation of state when the Grüneisen Γ does not depend on the density. It may be an adequate description of the equation of state of the shocked medium, provided that the Grüneisen Γ is independent of density and the shock wave is strong. However, the shock waves produced by underground nuclear explosions are relatively weak during much of their hydrodynamic phase (see *Lamb* [1988]).

Heusinkveld also assumed a simple linear relation between D and u_1 of the form (6). However, the jump conditions (1), (2), and (3), the equation of state (A2), and the D vs. u_1 relation (6) are mutually inconsistent. For example, if one accepts the mass flux jump condition (1), the momentum jump condition (2), and the *ansatz* (A1), one finds that the energy jump condition (3) is inconsistent with a linear D vs. u_1 relation. Alternatively, if one accepts the D vs. u_1 relation (6), one is led to the Hugoniot (see *Zel'dovich and Raizer* [1967], p. 710)

$$p_H(V) = \frac{A^2(V_0 - V)}{[BV - (B-1)V_0]^2} ,$$ (A3)

27

which is inconsistent with the jump conditions (1), (2), and (3) and the equation of state (A2).

Heusinkveld's model gives expressions for the shock speed, the radius vs. time curve, and the post-shock pressure, post-shock particle speed, and post-shock internal energy that are qualitatively different from the expressions given by the model of § 2. For example, by equating the pressure given by expression (A2) with the post-shock pressure given by the momentum jump condition (2) and making use of the *ansatz* (A1), Heusinkveld obtained a quadratic equation involving the shock speed. The solution of this equation is

$$D_H = \frac{A}{2}\left[1 + \left(1 + \frac{g^3}{R^3}\right)^{1/2}\right],$$
(A4)

where

$$g \equiv \left(\frac{3\Gamma f_H BW}{\pi \rho_0 A^2}\right)^{1/3}$$
(A5)

is a characteristic length, analogous to the characteristic length L defined in equation (8). Expression (A4) is qualitatively different from equation (9), the relationship predicted by the model of § 2. The radius vs. time curve predicted by Heusinkveld's model can be obtained by numerically integrating equation (A4).[2]

Even though the model of § 2 is self-consistent whereas Heusinkveld's model is not, both are approximate. Thus, their usefulness is best evaluated by comparing their predictions with data from nuclear tests and/or numerical simulations. We show here comparisons of the predictions of the two models with data from numerical simulations for three reasons. First, the initial conditions of these simulations approach that of point explosions, a simple case that the two models each describe. Second, we lack detailed knowledge of the conditions under which the nuclear test data were obtained (see § 4). Third, the simulations have reportedly been validated by extensive comparison with data from underground nuclear tests.

In comparing the two models with the results of simulations, we wish to make a consistent choice of model parameters. We do this by forcing agreement between the two models at the beginning of the explosion, as follows. At early times, the radius vs. time curve given by Heusinkveld's model displays the $t^{2/5}$ dependence characteristic of a strong, self-similar shock wave, that is,

$$R_H(t) = \left(\frac{75\Gamma f_H BW}{16\pi \rho_0}\right)^{1/5} t^{2/5}.$$
(A6)

---

[2] Although Heusinkveld assumed a simple linear D vs u_1 relation, an arbitrary D vs u_1 relation can be treated to any desired accuracy by using a piecewise-linear approximation, as described in § 2.

On comparing this curve with the early time curve given by the model of § 2, namely,

$$R(t) = \left(\frac{75 f B^2 W}{16 \pi \rho_0} \right)^{1/5} t^{2/5} , \tag{A7}$$

we see that if Γf_H is set equal to fB, the two models will give identical results at the beginning of the explosion. In the comparisons that follow, we do this.

Figures A1 and A2 compare the radius vs. time curves predicted by the two models for explosions in quartz and wet tuff with the data from simulated explosions in the same media that were described in § 2. For the explosion in quartz, we used $\Gamma f_H = 0.325$, whereas for wet tuff we used $\Gamma f_H = 0.299$. For comparison, Heusinkveld obtained $\Gamma f_H = 0.78$ for explosions in alluvium and wet tuff and 1.03 for explosions in granite by fitting his model to the particle speed data of *Perret and Bass* [1975] at relatively late times; had we used these values in the comparisons, the discrepancies between Heusinkveld's model and the simulations would have been much greater. Although the radius vs. time curves are integrals of the shock speeds predicted by the models and hence tend to smooth out differences, the curve predicted by the analytical model of § 2 agrees better with the simulations than does the curve predicted by Heusinkveld's model.

Additional and more decisive comparisons can be made between the post-shock pressures and particle speeds given by the models. On substituting equation (A4) into the D vs. u_1 relation (6), one finds that Heusinkveld's model predicts the post-shock particle speed

$$u_1^H = \frac{A}{2B} \left[\left(1 + \frac{3 \Gamma f_H B W}{\pi \rho_0 A^2 R^3} \right)^{1/2} - 1 \right] . \tag{A8}$$

At small radii, equation (A8) becomes

$$u_1^H \approx \left(\frac{3 \Gamma f_H W}{4 \pi \rho_0 B R^3} \right)^{1/2} , \quad R \ll g . \tag{A9}$$

Thus, u_1^H has the same R-dependence at small radii as that given by the *ansatz* (5) of § 2, once Γf_H has been set equal to fB. However, at large radii the post-shock particle speed predicted by Heusinkveld's model scales with radius according to

$$u_1^H \approx \frac{3 \Gamma f_H W}{\pi \rho_0 A R^3} , \quad R \gg g . \tag{A10}$$

Figures A3 and A4 compare the post-shock particle speeds predicted by the two models with those derived from the simulated explosions in quartz and wet tuff. The $R^{-3/2}$-dependence predicted by the model of § 2 agrees much better with the particle speed data at late times than does the R^{-3} dependence predicted by Heusinkveld's model. In

29

particular, there is no evidence of the break in the slope of the u_1 vs. R curve at $R \approx g$ that is predicted by Heusinkveld's model.

The post-shock pressure predicted by Heusinkveld's model is given by equations (A1) and (A2), and is

$$p_1 = \frac{3\Gamma f_H W}{4\pi R^3} . \tag{A11}$$

In contrast, the model of § 2 predicts that the post-shock pressure falls off as R^{-3} for $R \ll L$, but is proportional to $R^{-3/2}$ for $R \gg L$ (See eq. [23]). Figures A5 and A6 show that the pressure curves derived from the simulations show such a break at about the right radius, demonstrating that the model of § 2 is in better agreement with the simulations than is Heusinkveld's model.

Perret and Bass [1975] show that pressure data from explosions in several geologic media is well fit by $R^{-2.96}$ out to distances of $8\,m/W^{1/3}$, at which point a clear break occurs. At distances beyond this break, the data are better described by $R^{-1.75}$. This large R behavior is more in keeping with the analytical model of § 2 than the R^{-3} dependence at all distances predicted by Heusinkveld's model.

The predictions of the two models differ significantly well before the assumptions of the model discussed in § 2 become invalid. As discussed in § 4, the hydrodynamic phase extends at least out to the radius at which the post-shock pressure has fallen to 15 GPa. Obviously, the ambient pressure of 20 MPa can be neglected throughout the hydrodynamic phase. As noted in § 2, the ambient specific internal energy can be neglected for particle speeds greater than 0.1 km/s; Figures A3 and A4 show that the post-shock particle speed is actually 1 km/s or greater throughout the hydrodynamic phase. Figures A1–A6 show that the differences between the two models are already significant at 10 meters, and increase dramatically at larger radii, whereas the post-shock pressure falls to 15 GPa at 25 meters in quartz and 22 meters in wet tuff. At 25 meters in quartz, the peak particle speed predicted by the model we discuss falls right on the curve predicted by the numerical simulation, and is 2.5 times larger than the peak particle speed predicted by Heusinkveld's model, which is far below the curve predicted by the simulation.

These comparisons show that the model of § 2, which fully incorporates the Rankine-Hugoniot jump conditions and does not assume any particular equation of state, also agrees better with the radius vs. time curves and the post-shock particle speed and pressure data derived from the simulated explosions than does the model suggested by Heusinkveld.

REFERENCES

Ahrens, T. J., and V. G. Gregson, Jr., Shock compression of crustal rocks: data for quartz, calcite, and plagioclase rocks, *J. Geophys. Res.*, *69*, 4839–4874, 1964.

Al'tshuler, L. V., N. N. Kalitkin, L. V. Kuz'mina, and B. S. Chekin, Shock adiabats for ultrahigh pressures, *Sov. Phys. JETP*, *45*, 167–171, 1977.

Bass, R. C., and Larsen, G. E., Shock propagation in several geologic materials of interest in hydrodynamic yield determinations, *Sandia National Laboratory, Rep. SAND77-0402*, March 1977.

Callen, B. W., F. K. Lamb, and J. D. Sullivan, Insensitive interval in the evolution of shock waves from explosions, in *Shock Compression of Condensed Matter-1989*, S. C. Schmidt, J. N. Johnson, and L. W. Davison, eds., pp. 241–244, Selsevier Science Pubs., Amsterdam, 1990a.

Callen, B. W., F. K. Lamb, and J. D. Sullivan, Hydrodynamic determination of the yield of underground nuclear explosions, in *Proc. 12th Annual DARPA/GL Seismic Research Symposium*, pp. 241–250, Air Force Geophysics Laboratory, Hanscom Air Force Base, Mass., 1990b. (Also *Dept. of Physics, University of Illinois at Urbana-Champaign, Rep. P/90/9/116*, September 1990.) GL-TR-90-0212, ADA226635

Chung, D. H., and G. Simmons, Pressure derivatives of the elastic properties of polycrystalline quartz and rutile, *Earth Planet. Sci. Lett.*, *6*, 134–138, 1969.

Cox, A. N., R. R. Brownlee, and D. D. Eilers, Time-dependent method for computation of radiation diffusion and hydrodynamics, *Ap. J.*, *144*, 1024–1037, 1966.

Dahlman, O., and H. Israelson, *Monitoring Underground Nuclear Explosions*, p. 398. Elsevier, Amsterdam, 1977.

Glasstone, S., and P. J. Dolan, *Effects of Nuclear Weapons* (3rd ed.), U. S. Government Printing Office, Washington, 1977.

Grady, D. E., W. J. Murri, and G. R. Fowles, Quartz to stishovite: wave propagation in the mixed phase region, *J. Geophys. Res.* *79*, 332–338, 1974.

Heusinkveld, M., and F. Holzer, Method of continuous shock front position measurement, *Rev. Sci. Inst.*, *35*, 1105–1107, 1964.

Heusinkveld, M., Analysis of SLIFER data from underground nuclear explosions, *Lawrence Livermore National Laboratory, Rep. UCRL-52648*, 1979.

Heusinkveld, M., Analysis of shock wave arrival time from underground explosions, *J. Geophys. Res.*, *87*, 1891–1898, 1982.

Heusinkveld, M., Shock arrival times in granite, *Lawrence Livermore National Laboratory, Earth Sciences Department Mem. 0004A*, 30 October 1986.

Holzer, F., Measurements and calculations of peak shock-wave parameters from underground nuclear detonations, *J. Geophys. Res.*, *70*, 893–905, 1965.

Johnson, G. W., G. H. Higgins, and C. E. Violet, Underground nuclear detonations, *J. Geophys. Res.*, *64*, 1457–1470, 1959.

Jones, A. H., W. M. Isbell, F. H. Shipman, R. D. Perkins, S. J. Green, and C. J. Maiden, Material properties measurements for selected materials, Interim report, *Contract NAS2-3427*, General Motors Technical Center, Warren, Mich., April 1968.

King, D. S., B. E. Freeman, D. D. Eilers, and J. D. Johnson, The effective yield of a nuclear explosion in a small cavity in geologic material, *J. Geophys. Res.*, *94*, 12375–12385, 1989.

Lamb, F. K., An approximate solution for ground shock propagation, *University of Illinois Program in Arms Control, Disarmament, and International Security, Rep. WP-2-87-2*, February 1987.

Lamb, F. K., Monitoring yields of underground nuclear tests using hydrodynamic methods, in *Nuclear Arms Technologies in the 1990s*, D. Schroeer and D. Hafemeister, eds., pp. 109–148, American Institute of Physics, New York, 1988.

Lamb, F. K., B. W. Callen, and J. D. Sullivan, Insensitive interval in the evolution of shock waves from underground nuclear explosions, in *Proc. 11th Annual DARPA/AFGL Seismic Research Symposium*, Air Force Geophysics Laboratory, Hanscom Air Force Base, Mass., 1989. (' Dept. of Physics, University of Illinois at Urbana-Champaign, *Rep. P/89/5/77* 1989.) GL-TR-90-0301, ADA229228

Lamb, F. K., B. W. Callen, and J. D. Sullivan, Insensitive interval in the evolution of shock waves from underground nuclear explosions, to be submitted to *J. Geophys. Res.*, 1991a.

Lamb, F. K., B. W. Callen, and J. D. Sullivan, Scaling of shock waves from underground nuclear explosions, to be submitted to *J. Geophys. Res.*, 1991b.

Lamb, F. K., B. W. Callen, and J. D. Sullivan, Yield estimation using shock wave methods, to appear in *Explosion Source Phenomenolgy*, S. R. Taylor, P. G. Richards, and H. J. Patton, eds., American Geophysical Union, Washington, D. C., 1991c.

Landau, L. D., and E. M. Lifshitz, *Fluid Mechanics* (2nd ed.), Pergamon, New York, 1987.

Mathews, J., and R. L. Walker, *Mathematical Methods of Physics* (2nd ed.), W. A. Benjamin, New York, 1970.

McQueen, R., J. N. Fritz, and J. W. Hopson, High-pressure equation of state of SiO_2, *M-6 Prog. Rep. M-6-200*, pp. 78–136, Los Alamos National Laboratory, Los Alamos, N. M., January–March 1977.

Moran, B., and H. C. Goldwire, Jr., Effect of source modelling on the inferred yield from an underground nuclear explosion, in *Shock Compression of Condensed Matter-1989*, S. C. Schmidt, J. N. Johnson, and L. W. Davison, eds., pp. 645–648, North-Holland, Amsterdam, 1990.

Moss, W. C., A method to estimate the yield of an underground nuclear explosion, *J. Appl. Phys.*, *63*, 4771–4773, 1988.

Nuckolls, J. H., A computer calculation of Rainier (the first 100 milliseconds) in *Proc. Second Plowshare Symposium*, May 13–15, 1959, San Francisco, California. Part I. Phenomenology of Underground Nuclear Explosions, *University of California Radiation Laboratory, Rep. UCRL-5675*, pp. 120–134, 1959.

Perret, W. R., and R. C. Bass, Free-field ground motion induced by underground explosions, *Sandia National Laboratory, Rep. SAND74-0252*, February 1975.

Ragan, C. E., III, Shock-wave experiments at threefold compression, *Phys. Rev. A, 29*, 1391–1402, 1984.

Sedov, L. I., The motion of air in a strong explosion, *Akademiya nauk SSSR, Doklady, 52*, [in Russian], 17–20, 1946.

Sedov, L. I., *Similarity and Dimensional Methods in Mechanics*, Academic Press, New York, 1959 [English translation].

Taylor, G. I., The formation of a blast wave by a very intense explosion. I. Theoretical discussion, *Proc. Roy. Soc. (London), A201*, 159–174, 1950a.

Taylor, G. I., The formation of a blast wave by a very intense explosion. II. The atomic explosion of 1945, *Proc. Roy. Soc. (London), A201*, 175–186, 1950b.

U. S. Arms Control and Disarmament Agency, *Arms Control and Disarmament Agreements*, 1990a.

U. S. Arms Control and Disarmament Agency, *Treaty Between the United States of America and the Union of Soviet Socialist Republics on the Limitation of Underground Nuclear Weapons Tests and Treaty Between the United States of America and the Union of Soviet Socialist Republics on Underground Nuclear Explosions for Peaceful Purposes: Text of Treaties and Protocols*, 1990b.

U. S. Congress, Office of Technology Assessment, *Seismic Verification of Nuclear Testing Treaties*, OTA-ISC-361, U. S. Government Printing Office, Washington, D. C., pp. 129–139, May 1988.

U. S. Department of Energy, *Announced United States Nuclear Tests, July 1945 through December 1986*, NVO-209 (Rev. 7), Nevada Operations Office, January 1987.

U. S. Department of State, Bureau of Public Affairs, U. S. policy regarding limitations on nuclear testing, *Special Report No. 150*, August 1986.

U. S. Department of State, Bureau of Public Affairs, Verifying nuclear testing limitations: possible U. S.-Soviet cooperation, *Special Report No. 152*, August 1986.

U. S. Department of State, *Agreement Between the United States of America and the Union of Soviet Socialist Republics on the Conduct of a Joint Verification Experiment*, May 1988.

Virchow, C. F., G. E. Conrad, D. M. Holt, and E. K. Hodson, Microprocessor-controlled time domain reflectometer for dynamic shock position measurements, *Rev. Sci. Inst., 51*, 642–646, 1980.

Wackerle, J., Shock-wave compression of quartz, *J. Appl. Phys.*, *33*, 922–937, 1962.

Zel'dovich, Ya. B., and Yu. P. Raizer, *Physics of Shock Waves and High-Temperature Hydrodynamic Phenomena*, Academic Press, New York, 1967 [English translation].

Figure Captions

Fig. 1.—Dimensionless energy partition factor f as a function of Grüneisen coefficient Γ for a strong point explosion in a medium obeying a Mie-Grüneisen equation of state.

Fig. 2.—Hugoniot data for SiO_2 and two of the representations used in calculations described in the text. The solid line shows the piecewise-linear approximation to the full Hugoniot while the dashed line shows a simple linear approximation to the high-pressure portion of the Hugoniot.

Fig. 3.—Expanded view of SiO_2 Hugoniot data at low pressures and three representations used in calculations described in the text. The solid line shows the piecewise-linear approximation to the full Hugoniot while the dashed line shows a simple linear approximation to the high-pressure portion of the Hugoniot. The latter is clearly inaccurate at low particle speeds. The dash-dotted segment at low u_1 is similar to the approximate Hugoniot used by King et al. [1989] and replaces the corresponding section of the piecewise-linear Hugoniot when comparisons are made with the numerical simulations of D. Eilers et al. Also shown is the isobar at 15 GPa, the pressure we have adopted as marking the end of the hydrodynamic phase.

Fig. 4.—Hugoniot data for wet tuff [King et al., 1989] and two representations used in calculations described in the text. The solid line shows our piecewise-linear approximation to the full Hugoniot, while the dashed line shows the simple linear approximation to the high-pressure portion of the Hugoniot. Also shown is the isobar at 15 GPa, the pressure we have adopted as marking the end of the hydrodynamic phase.

Fig. 5.—Peak particle speed u_1 vs. shock front radius R for a 100 kt explosion in SiO_2, from a numerical simulation by D. Eilers et al. (private communication, 1987), compared with the peak particle speed predicted by the analytical model (solid line). The analytical model describes the data quite well over two decades of particle speed, showing that the energy partition ansatz (eq. [5]) is relatively accurate.

Fig. 6.—Peak particle speed u_1 vs. shock front radius R for a 100 kt explosion in wet tuff, from a numerical simulation by D. Eilers et al. (private communication, 1987), compared with the peak particle speed predicted by the analytical model (solid line). Again, the analytical model describes the data quite well over two decades of particle speed, showing that the energy partition ansatz (eq. [5]) is relatively accurate.

Fig. 7.—Comparison of shock front radius vs. time curves predicted by the analytical model with radius vs. time data from the numerical simulation of a 100 kt explosion in

36

SiO_2 by D. Eilers et al. (private communication, 1987). *Left panel*: Predicted radii as functions of time. *Right panel*: Relative difference between radii predicted from the SiO_2 simulation and from the analytical model. The dash-dotted lines show the results when the piecewise-linear representation of the full Hugoniot (see Figs. 2 and 3) is used in the analytical model; the dashed lines show the results when the simple linear approximation to the high-pressure portion of the Hugoniot (again see Figs. 2 and 3) is used.

Fig. 8.--Comparison of shock front radius vs. time curves predicted by the analytical model with radius vs. time data from the numerical simulation of a 100 kt explosion in wet tuff by D. Eilers et al. (private communication, 1987). *Left panel*: Predicted radii as functions of time. *Right panel*: Relative difference between radii predicted from the SiO_2 simulation and from the analytical model. The dash-dotted lines show the results when the piecewise-linear representation of the full Hugoniot (see Fig. 4) is used in the analytical model; the dashed lines show the results when the simple linear approximation to the high-pressure portion of the Hugoniot (again see Fig. 4) is used.

Fig. 9.--Comparison of shock front radius vs. time curves predicted by the analytical model with radius vs. time data from *Piledriver*, a 62 kt explosion in granite. The arrow in each panel marks the radius at which the peak pressure drops to 15 GPa, which we have adopted as the end of the hydrodynamic phase. *Left panel*: Predicted and measured radii as functions of time. *Right panel*: Relative difference between measured and predicted radii. The solid lines show the results when the piecewise-linear representation of the full Hugoniot (see Figs. 2 and 3) is used in the analytical model; the dashed lines show the results when the simple linear approximation to the high-pressure portion of the Hugoniot (again see Figs. 2 and 3) is used. When the piecewise-linear Hugoniot is used, the radii predicted by the analytical model differ from the measured radii by no more than 7% over the whole range of the data. The piecewise-linear representation of the Hugoniot is clearly superior to the simple linear after about 0.5 ms.

Fig. 10.--Hugoniot data for basalt from *Jones et al.* [1968] and *Ahrens and Gregson* [1964] and two representations used in calculations described in the text. The solid line shows the piecewise-linear representation of the full Hugoniot while the dashed line shows the simple linear approximation to the high-pressure portion of the Hugoniot.

Fig. 11.--Comparison of shock front radius vs. time curves predicted by the analytical model with radius vs. time data from *Cannikin*, an explosion in basalt with a yield of several Mt. The measurements have been scaled to show an apparent yield of 1 kt (see text). *Left panel*: Predicted and measured radii as functions of time. *Right panel*: Relative difference between measured and predicted radii. The solid lines show the results when the

37

piecewise-linear representation of the full Hugoniot (see Fig. 10) is used in the analytical model; the dashed lines show the results when the simple linear approximation to the high-pressure portion of the Hugoniot (again see Fig. 10) is used. The analytical model with the piecewise-linear Hugoniot predicts shock front radii that are within 3% of the measured radii over the full range of the data.

Fig. 12.—Comparison of shock front radius vs. time curves predicted by the analytical model with radius vs. time data from *Chiberta*, an explosion in wet tuff with a yield in the range 20–200 kt. The measurements have been scaled to show an apparent yield of 1 kt (see text). The arrow in each panel marks the radius at which the peak pressure drops to 15 GPa, which we have adopted as the end of the hydrodynamic phase. *Left panel*: Predicted and measured radii as functions of time. *Right panel*: Relative difference between measured and predicted radii. The solid lines show the results when the piecewise-linear representation of the full Hugoniot (see Fig. 4) is used in the analytical model; the dashed lines show the results when the simple linear approximation to the high-pressure portion of the Hugoniot (again see Fig. 4) is used. The analytical model with the piecewise-linear Hugoniot predicts shock front radii that are within 3% of the measured radii over the full range of the data.

Fig. 13.—Comparison of shock front radius vs. time curves predicted by the analytical model with radius vs. time data from *NTS-X*, assumed to be an explosion in wet tuff with a yield of 54.2 kt. The measurements have been scaled to show an apparent yield of 1 kt (see text). The arrow in each panel marks the radius at which the peak pressure drops to 15 GPa, which we have adopted as the end of the hydrodynamic phase. *Left panel*: Predicted and measured radii as functions of time. *Right panel*: Relative difference between measured and predicted radii. The solid lines show the results when the piecewise-linear representation of the full Hugoniot (see Fig. 4) is used in the analytical model; the dashed lines show the results when the simple linear approximation to the high-pressure portion of the Hugoniot (again see Fig. 4) is used. The analytical model with the piecewise-linear Hugoniot predicts shock front radii that are within 5% of the measured radii over the full range of the data.

Fig. A1. Comparison of the shock front radii predicted by the analytical model of § 2 (solid line) and the model of *Heusinkveld* [1982] (dashed line) with radius data from a numerical simulation of a 100 kt explosion in SiO_2 by D. Eilers et al. (private communication, 1987). The piecewise-linear representation of the SiO_2 Hugoniot shown in Figs. 2 and 3 was used in both models.

Fig. A2.—Comparison of the shock front radii predicted by the analytical model of § 2 (solid line) and the model of *Heusinkveld* [1982] (dashed line) with radius data from a numerical simulation of a 100 kt explosion in wet tuff by D. Eilers et al. (private communication, 1987). The piecewise-linear representation of the wet tuff Hugoniot shown in Fig. 4 was used in both models.

Fig. A3.—Comparison of the peak particle speed predicted by the analytical model of § 2 (solid line) and the model of *Heusinkveld* [1982] (dashed line) with peak particle speeds from a numerical simulation of a 100 kt explosion in SiO_2 by D. Eilers et al. (private communication, 1987). The piecewise-linear representation of the SiO_2 Hugoniot shown in Figs. 2 and 3 was used in the model of Heusinkveld. The peak particle speed predicted by the analytical model of § 2 is independent of the Hugoniot and scales as $R^{-3/2}$.

Fig. A4.—Comparison of the peak particle speed predicted by the analytical model of § 2 (solid line) and the model of *Heusinkveld* [1982] (dashed line) with peak particle speeds from a numerical simulation of a 100 kt explosion in wet tuff by D. Eilers et al. (private communication, 1987). The piecewise-linear representation of the wet tuff Hugoniot shown in Fig. 4 was used in the model of Heusinkveld. The peak particle speed predicted by the analytical model of § 2 is independent of the Hugoniot.

Fig. A5.—Comparison of the peak pressure predicted by the analytical model of § 2 (solid line) and the model of *Heusinkveld* [1982] (dashed line) with peak pressures from a numerical simulation of a 100 kt explosion in SiO_2 by D. Eilers et al. (private communication, 1987). The numerical results are more consistent with the $R^{-3/2}$ variation at large R predicted by the model of § 2 than with the R^{-3} variation predicted by the model of Heusinkveld.

Fig. A6.—Comparison of the peak pressure predicted by the analytical model of § 2 (solid line) and the model of *Heusinkveld* [1982] (dashed line) with peak pressures from a numerical simulation of a 100 kt explosion in wet tuff by D. Eilers et al. (private communication, 1987). Again, the numerical results are more consistent with the $R^{-3/2}$ variation at large R predicted by the model of § 2 than with the R^{-3} variation predicted by the model of Heusinkveld.

Tables

TABLE 1

Yield Estimates for *Piledriver*[a]

Model	Hugoniot	W_{est} (kt)	N	ΔR_{rms} (m)	$\Delta R_{rms}/W_{est}^{1/3}$
Analytical model	Linear SiO_2	37.6	22	0.785	0.234
Analytical model	Full SiO_2	62.5	25	0.312	0.079
Numerical simulation	King *et al.* SiO_2	63.4	24	0.349	0.088

[a] Yield estimates obtained by fitting the model or simulation to measurements made during the hydrodynamic phase of the explosion. W_{est} is the estimated yield, N is the number of data points used in the yield estimate, and ΔR_{rms} is the root-mean square difference between the measured and predicted shock front radii. The quantity $\Delta R_{rms}/W_{est}^{1/3}$ can be used to compare the quality of the fits for different explosions. The official yield of *Piledriver* was 62 kt [*U. S. Department of Energy*, 1987].

TABLE 2

Yield estimates for *Cannikin*[a]

Model	Hugoniot	W_{est} (kt)	N	ΔR_{rms} (m)	$\Delta R_{rms}/W_{est}^{1/3}$
Analytical model	Linear basalt	0.980	154	0.030	0.031
Analytical model	Full basalt	0.925	158	0.020	0.021
Numerical simulation	King *et al.* SiO_2	0.990	158	0.037	0.037

[a] Yield estimates obtained by fitting the model or simulation to measurements made during the hydrodynamic phase of the explosion. W_{est}, N, ΔR_{rms}, and $\Delta R_{rms}/W_{est}^{1/3}$ have the same meanings as in Table 1. The data for *Cannikin* have been scaled so that the apparent yield is 1 kt (see text).

TABLE 3

Yield Estimates for NTS-X[a]

Model	Hugoniot	W_{est} (kt)	N	ΔR_{rms} (m)	$\Delta R_{rms}/W_{est}^{1/3}$
Analytical model	Linear wet tuff	59.2	30	0.101	0.026
Analytical model	Full wet tuff	58.5	34	0.087	0.022
Numerical simulation	Full wet tuff	57.9	34	0.084	0.022

[a] Yield estimates obtained by fitting the model or simulation to measurements made during the hydrodynamic phase of the explosion. W_{est}, N, ΔR_{rms}, and $\Delta R_{rms}/W_{est}^{1/3}$ have the same meanings as in Table 1. The yield of NTS-X is given as 54.2 kt by *Heusinkveld* [1979].

TABLE 4

Yield Estimates for *Chiberta*[a]

Model	Hugoniot	W_{est} (kt)	N	ΔR_{rms} (m)	$\Delta R_{rms}/W_{est}^{1/3}$
Analytical model	Linear wet tuff	0.950	42	0.028	0.028
Analytical model	Full wet tuff	0.930	47	0.021	0.021
Numerical simulation	Full wet tuff	0.910	45	0.013	0.014

[a] Yield estimates obtained by fitting the model or simulation to measurements made during the hydrodynamic phase of the explosion. W_{est}, N, ΔR_{rms}, and $\Delta R_{rms}/W_{est}^{1/3}$ have the same meanings as in Table 1. The data for *Chiberta* were scaled so that the apparent yield is 1 kt (see text).

TABLE 5

Effect on Yield Estimates of Including Data from Outside the Hydrodynamic Phase[a]

Cutoff	NTS-X				Chiberta			
	W_{est} (kt)	N	ΔR_{rms} (m)	$\Delta R_{rms}/W_{est}^{-1/3}$	W_{est} (kt)	N	ΔR_{rms} (m)	$\Delta R_{rms}/W_{est}^{-1/3}$
15 GPa	58.5	34	0.087	0.022	0.930	47	0.021	0.021
7.5 GPa	66.4	83	0.271	0.067	0.970	81	0.037	0.037
4.6 GPa	71.5	141	0.320	0.077	0.995	104	0.044	0.044

[a] The results shown are for fits to data out to the radius at which the peak pressure predicted by the analytical model falls below the indicated cutoff value. According to the convention used in this work, the hydrodynamic phase ends when the peak pressure falls below 15 GPa. Thus, the fits with cutoff pressures below this value include data from beyond the hydrodynamic phase. W_{est}, N, ΔR_{rms}, and $\Delta R_{rms}/W_{est}^{-1/3}$ have the same meanings as in Table 1. The yield of NTS-X is given as 54.2 kt by Heusinkveld [1979]. The data from Chiberta have been scaled so that the apparent yield is 1 kt (see text).

43

Grüneisen Γ

Fig. 1

Fig. 2

Fig. 3

46

Wet Tuff

$p_1 = 15$ GPa

Fig. 4

Fig. 5

48

Fig. 6

49

Fig. 7

Fig. 8

Fig. 9

Basalt

$p_I = 15$ GPa

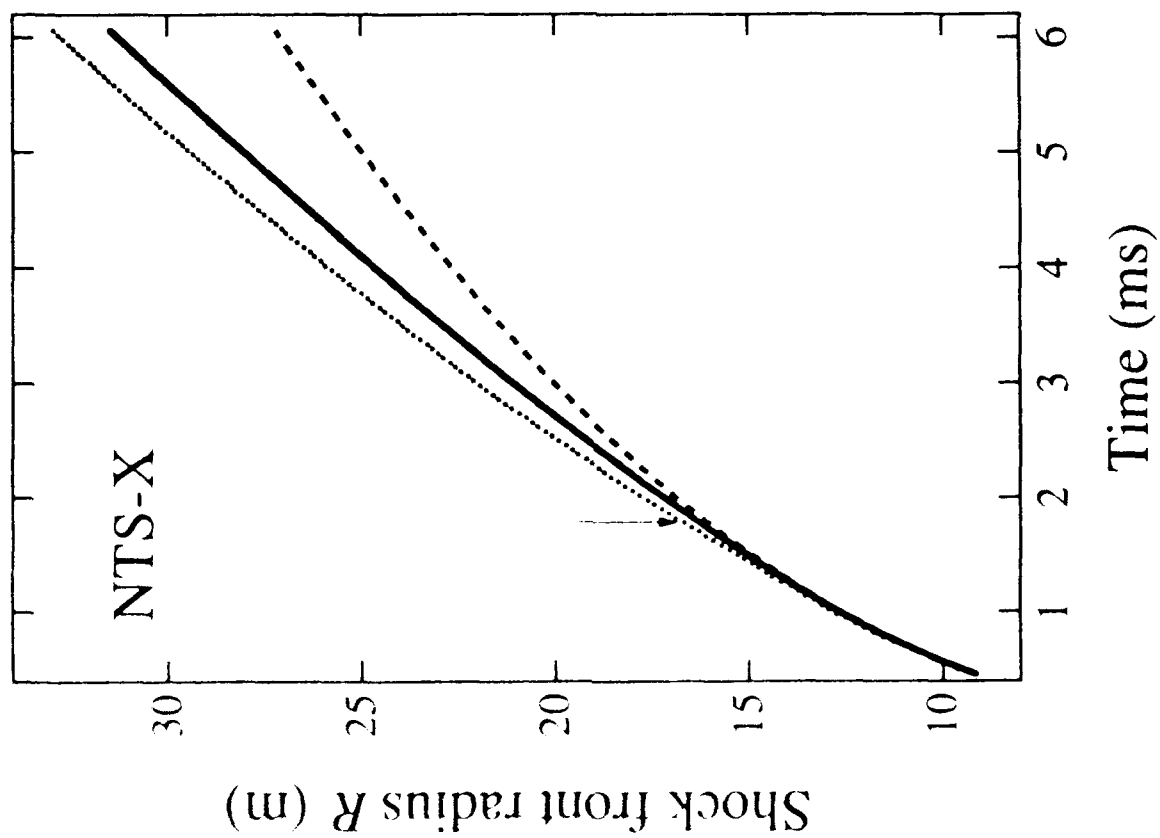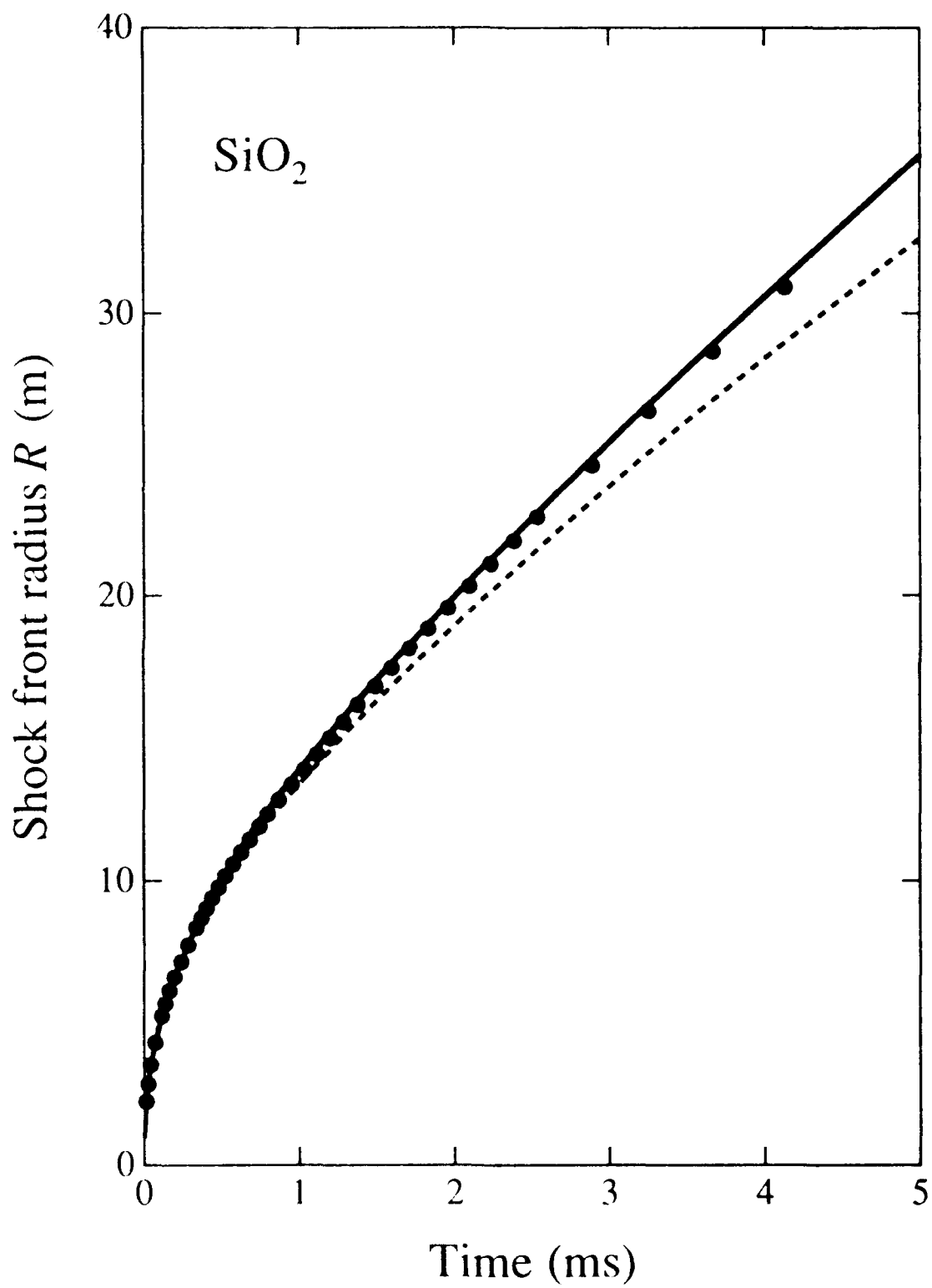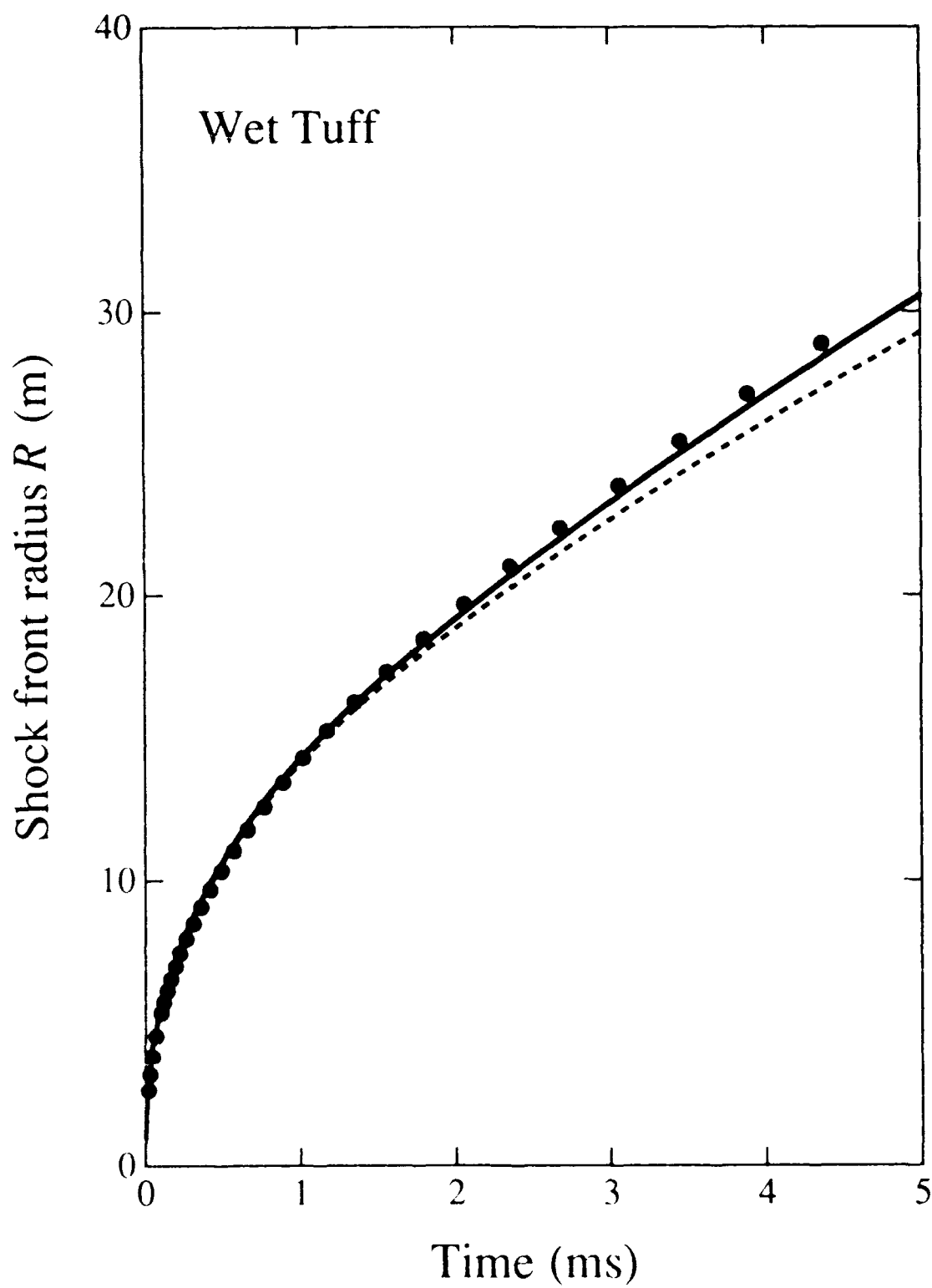Shock speed D (km/s)

Post-shock particle speed u_I (km/s)
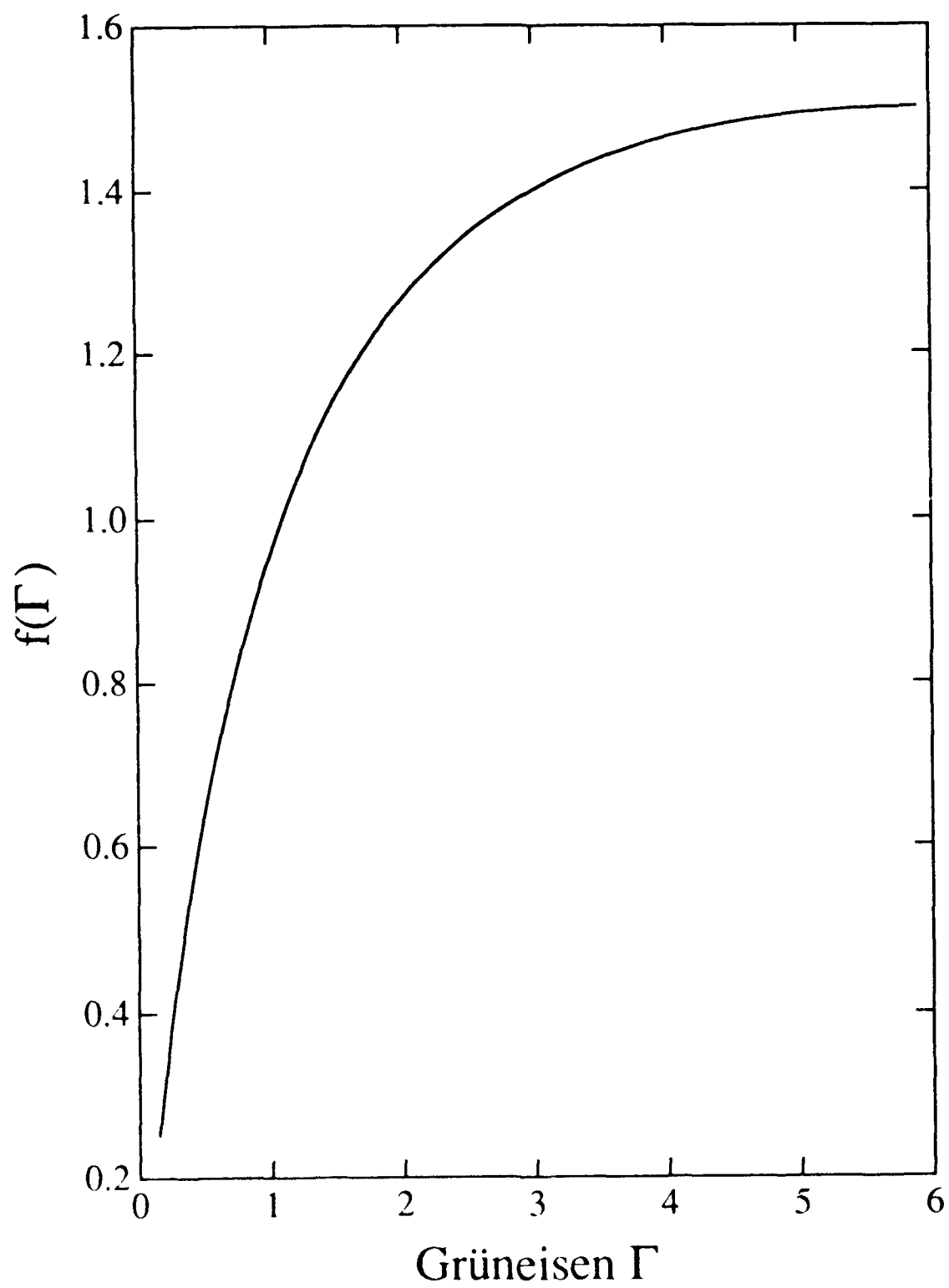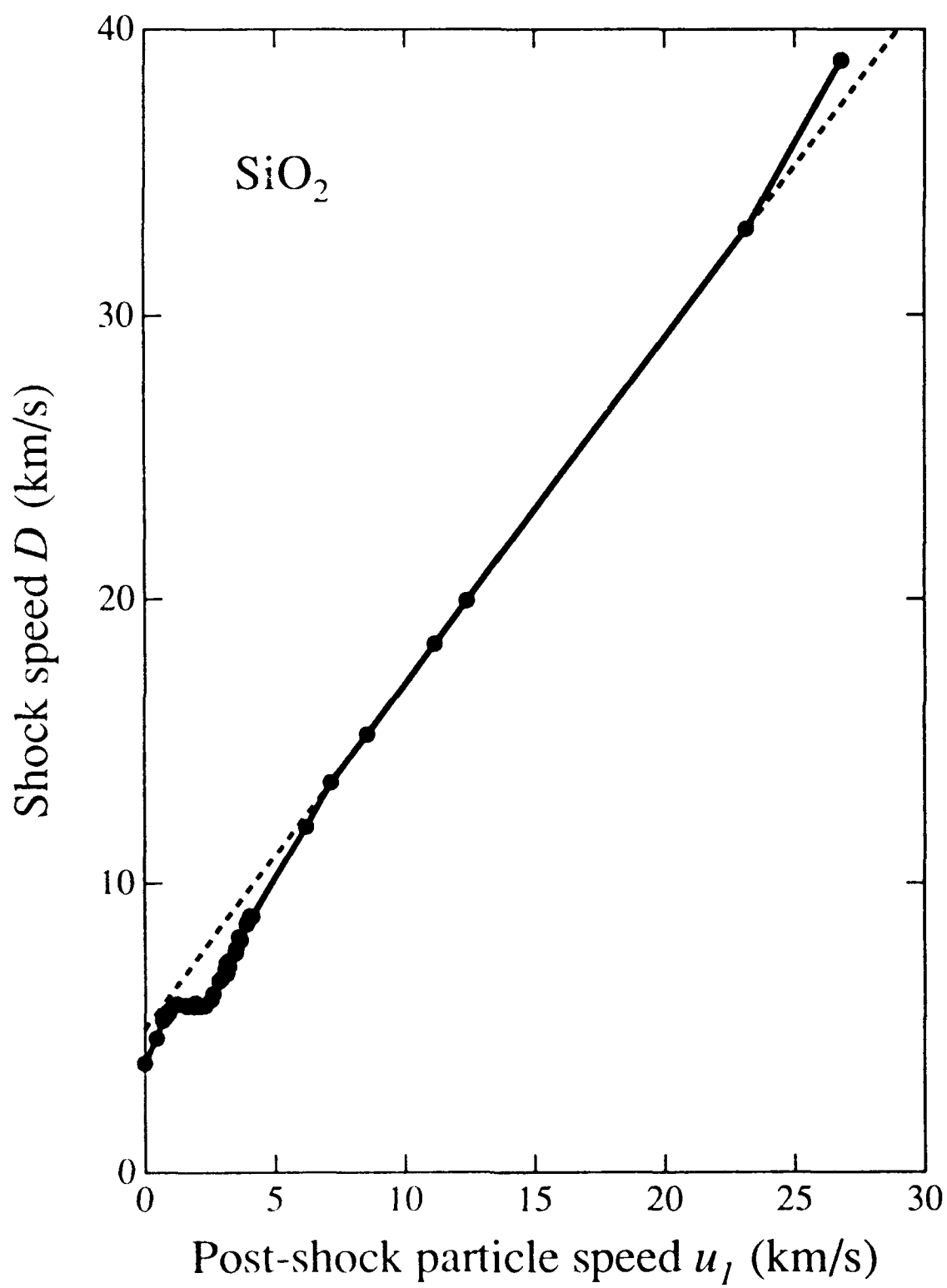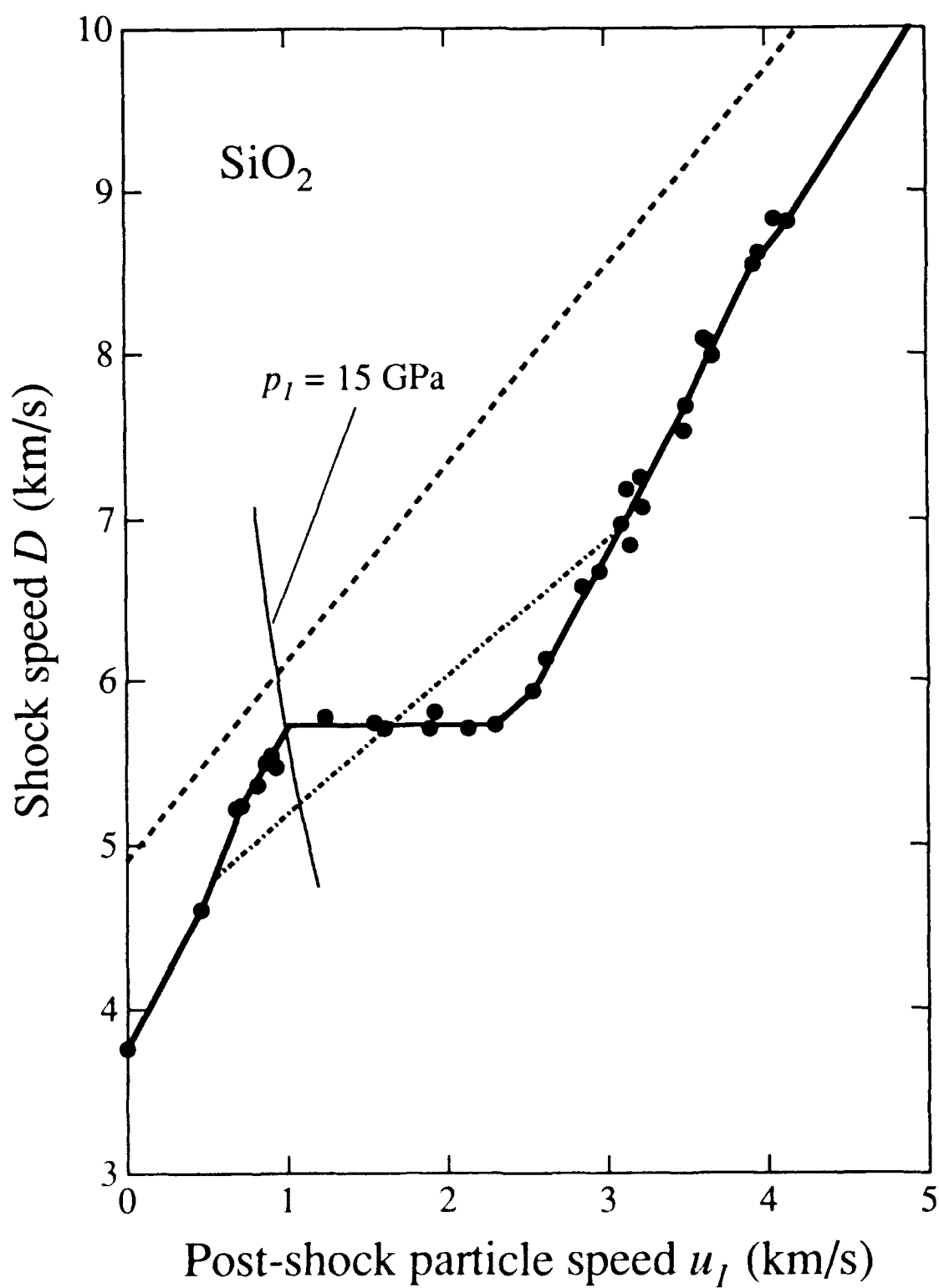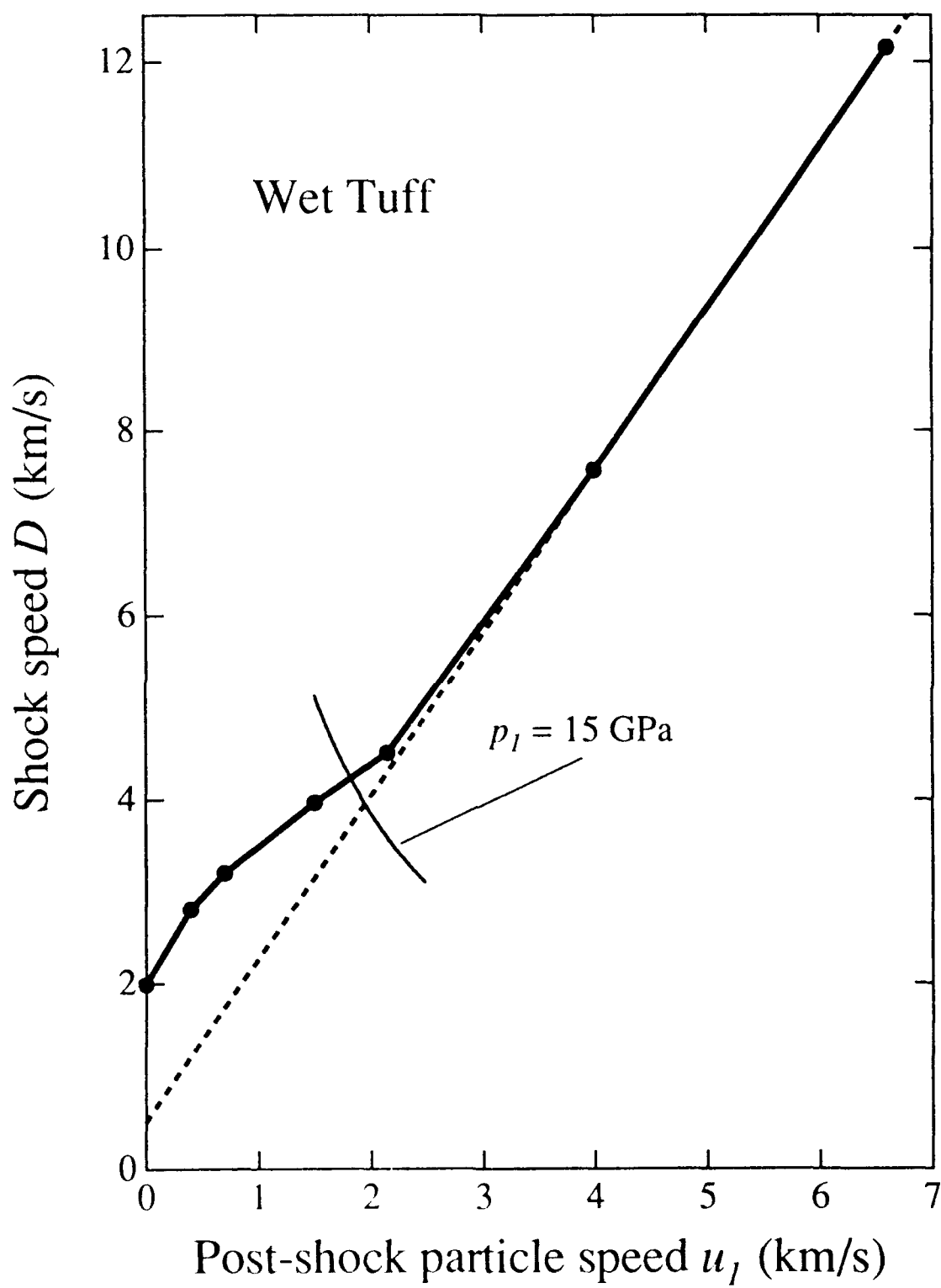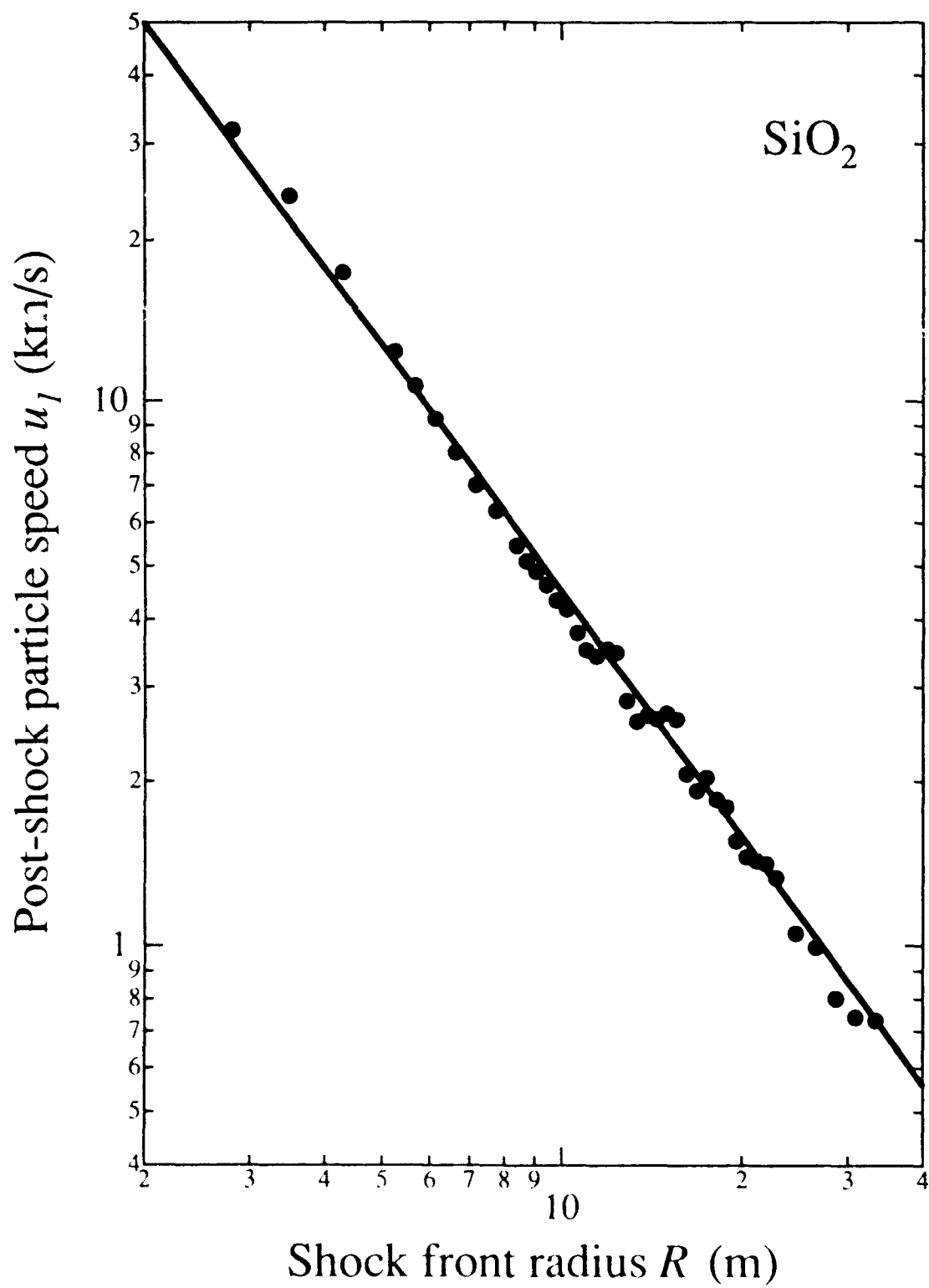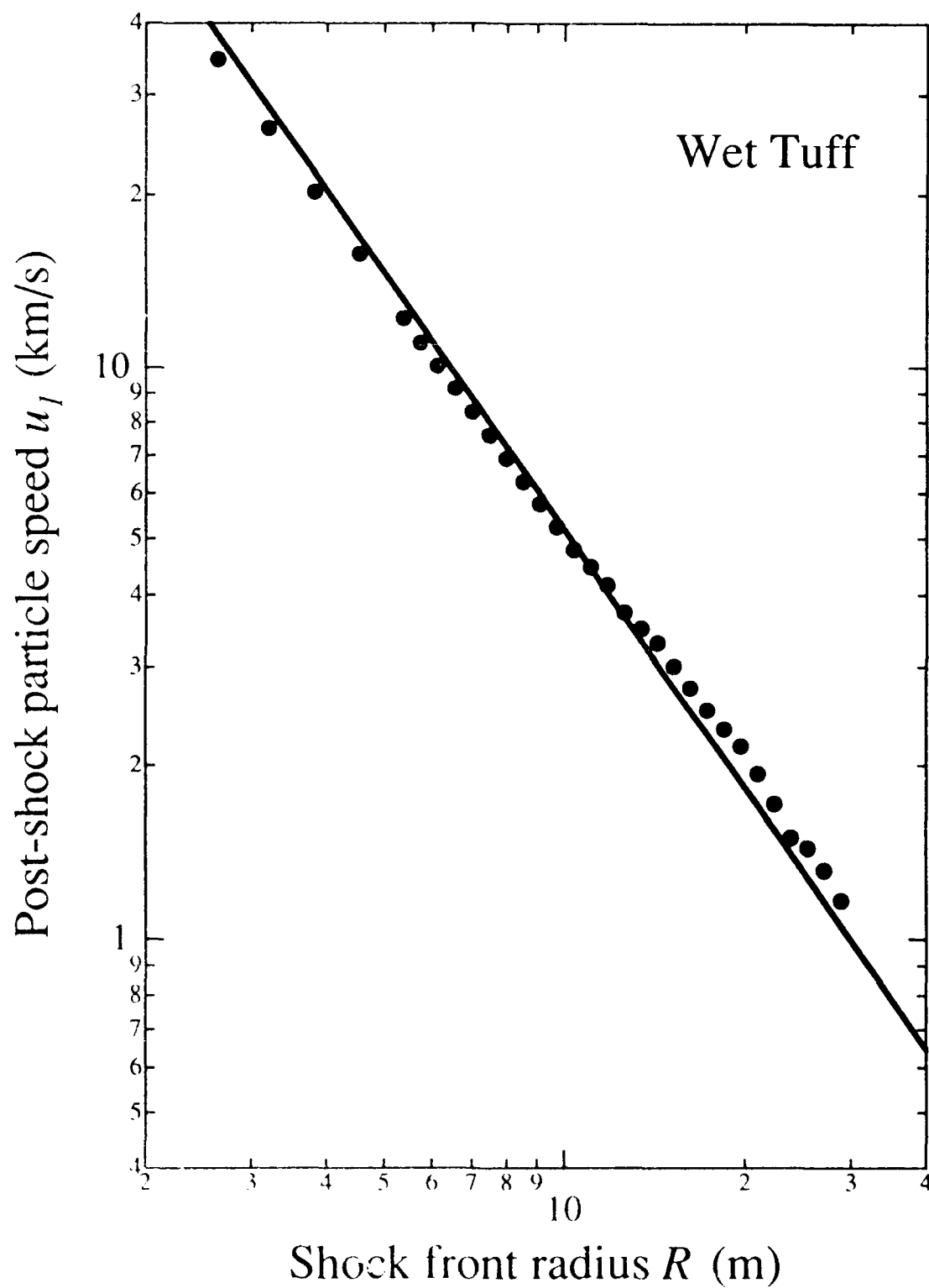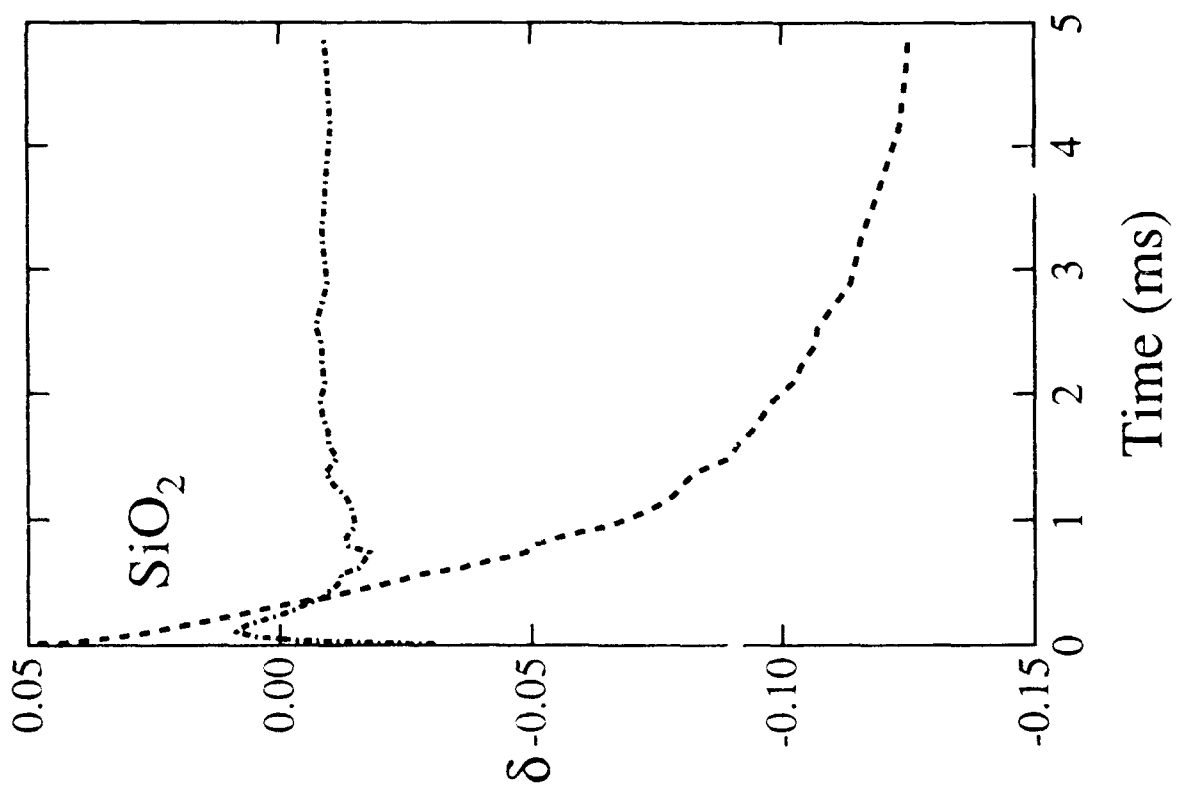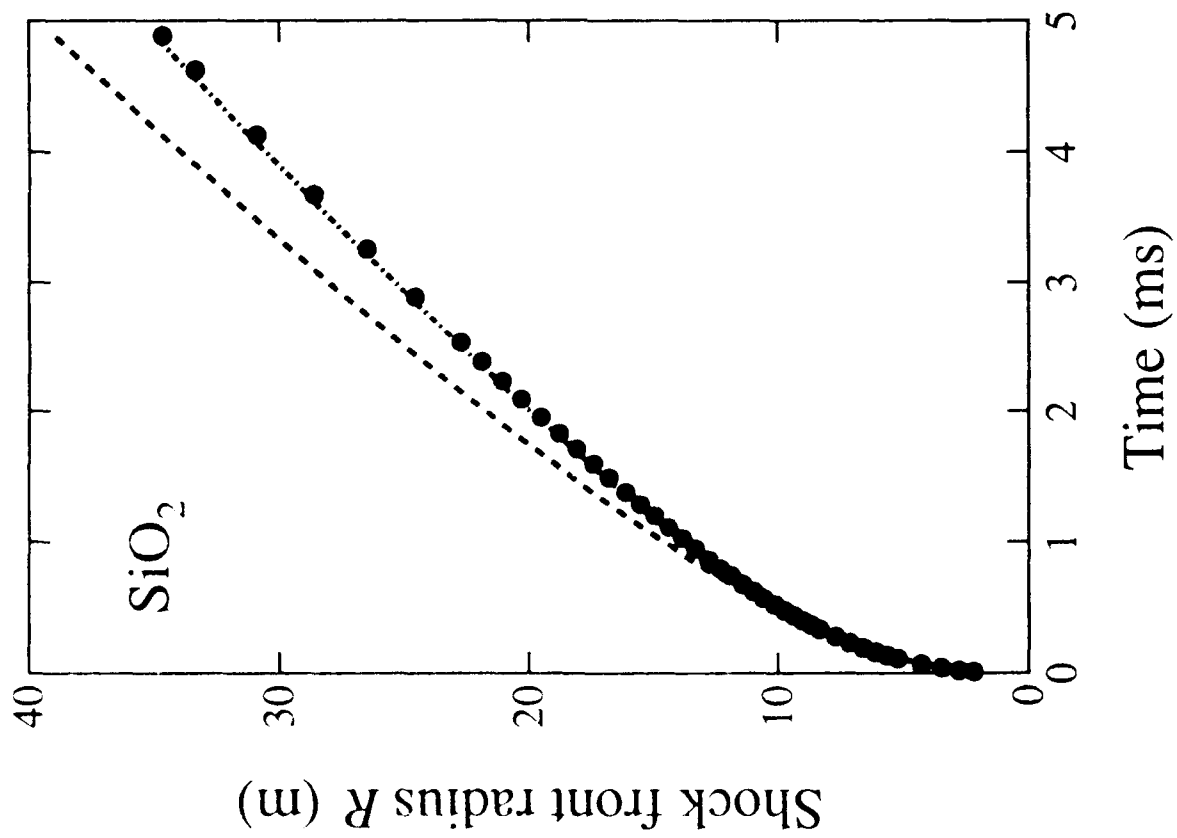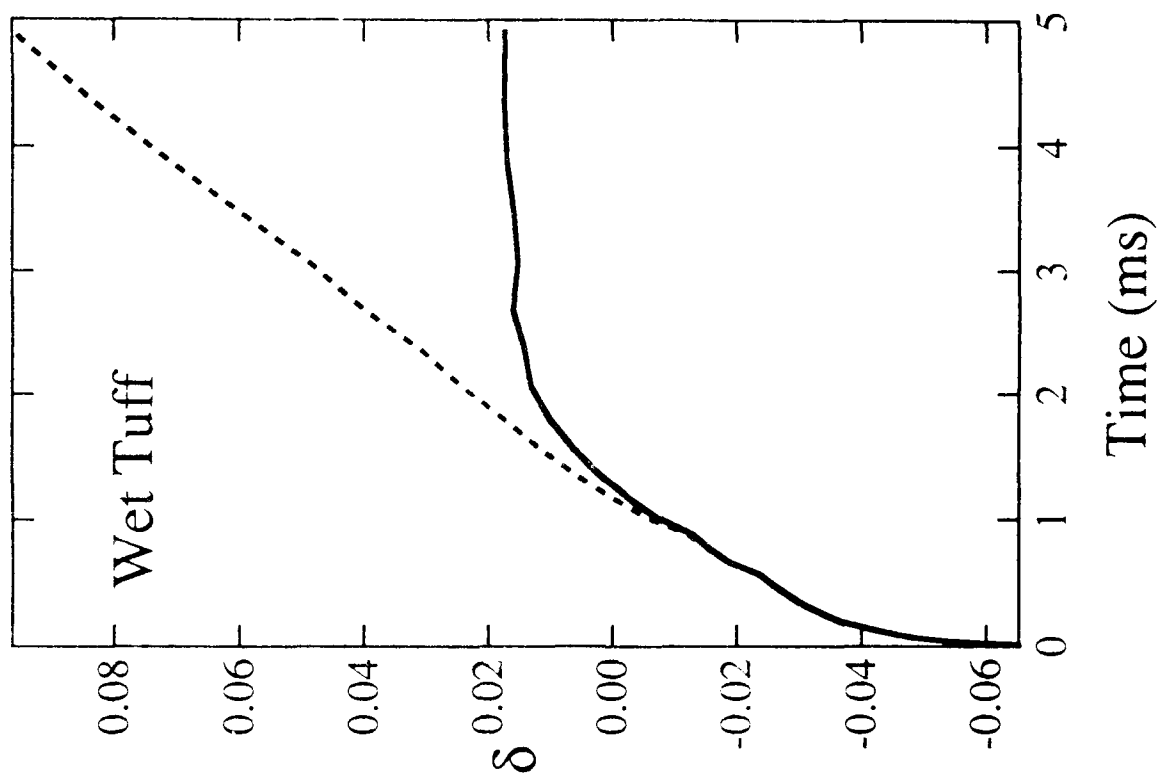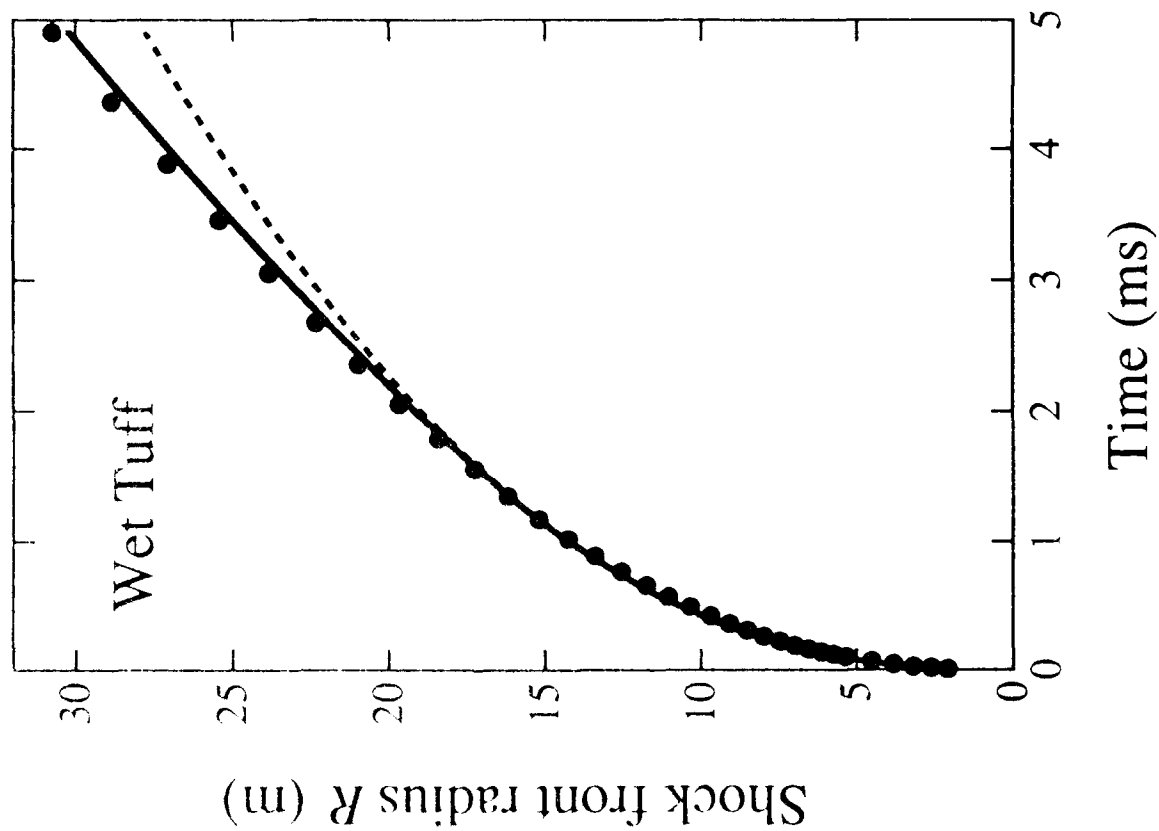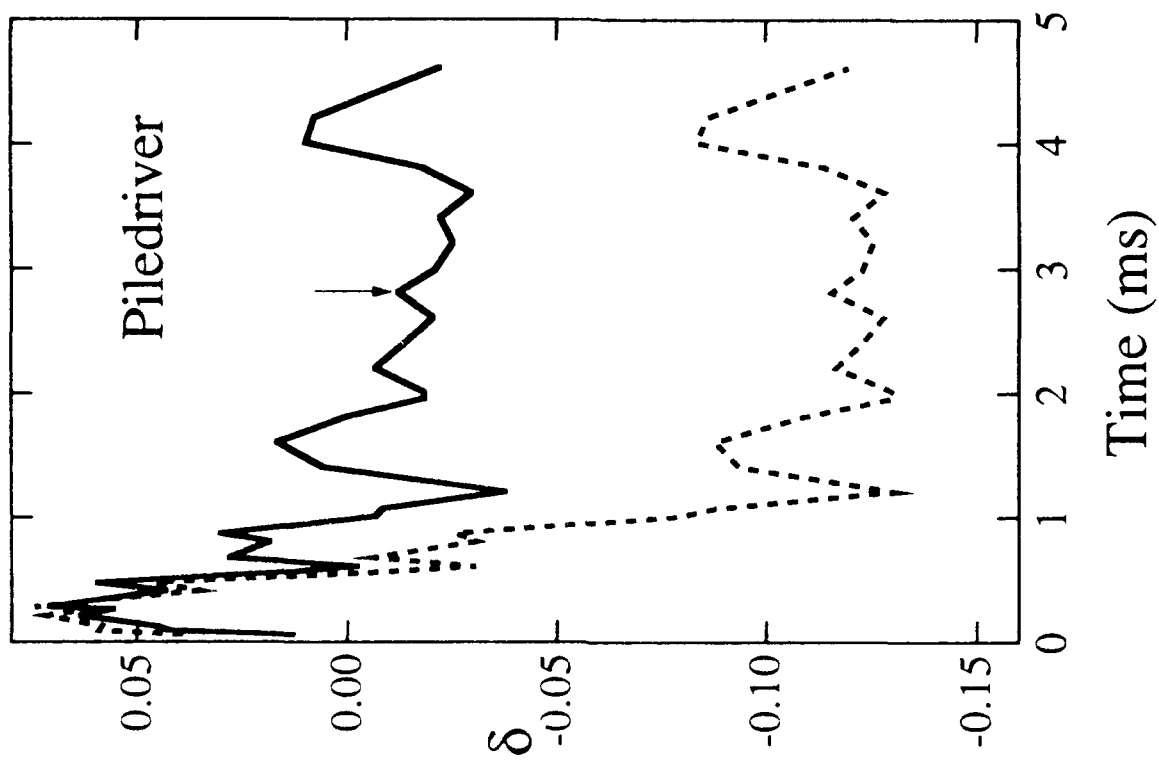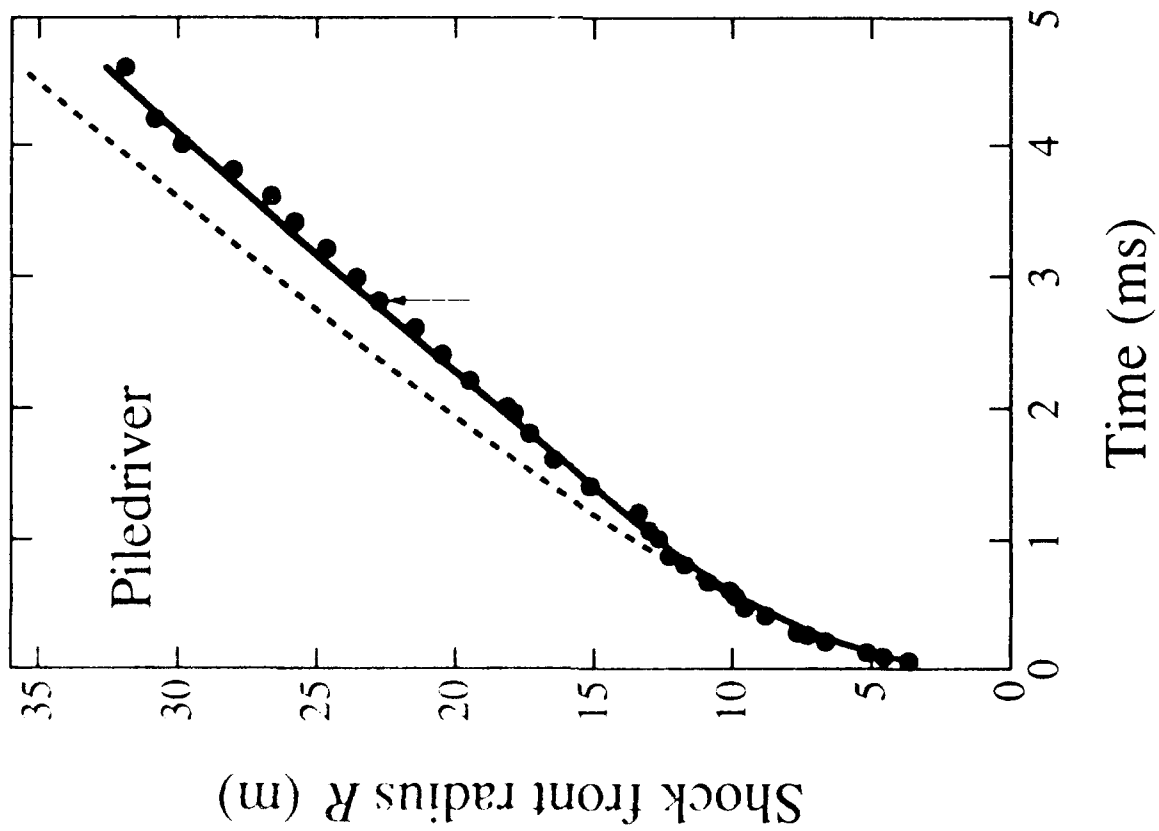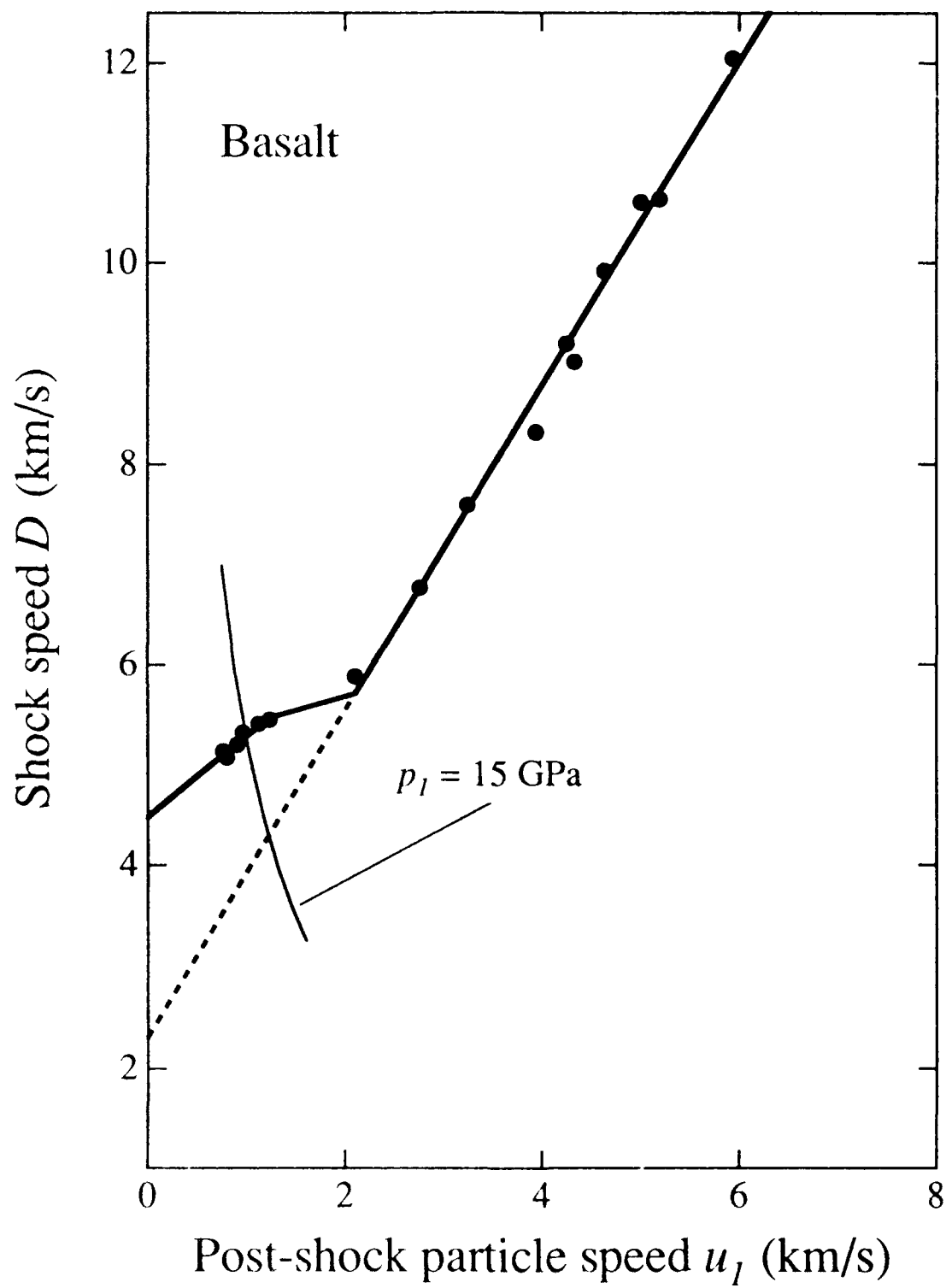
Fig. 10
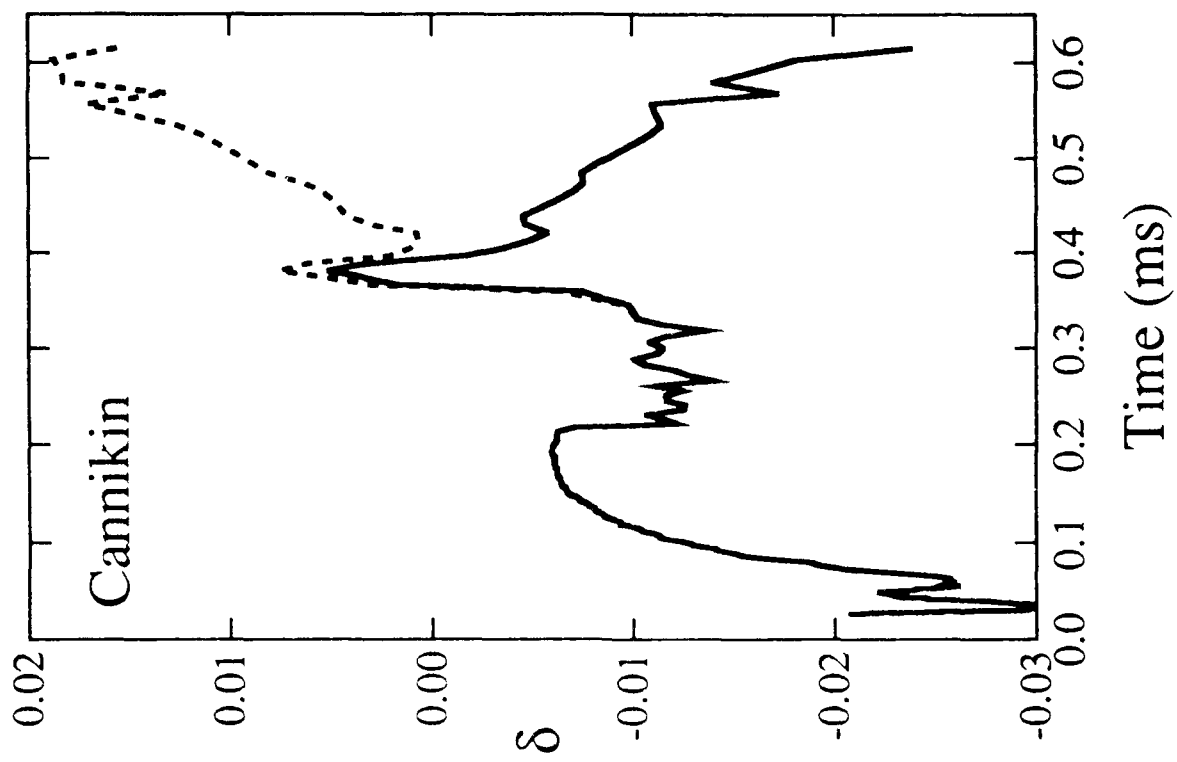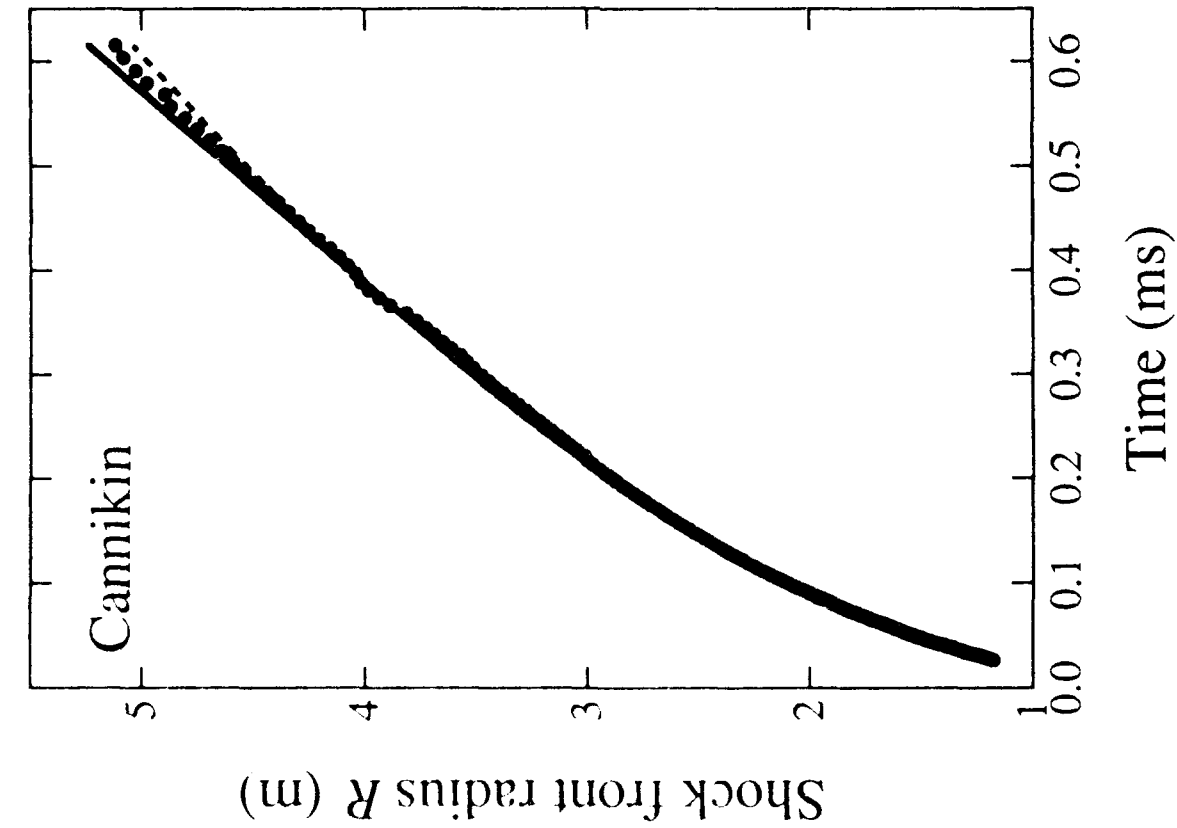
Fig. 11
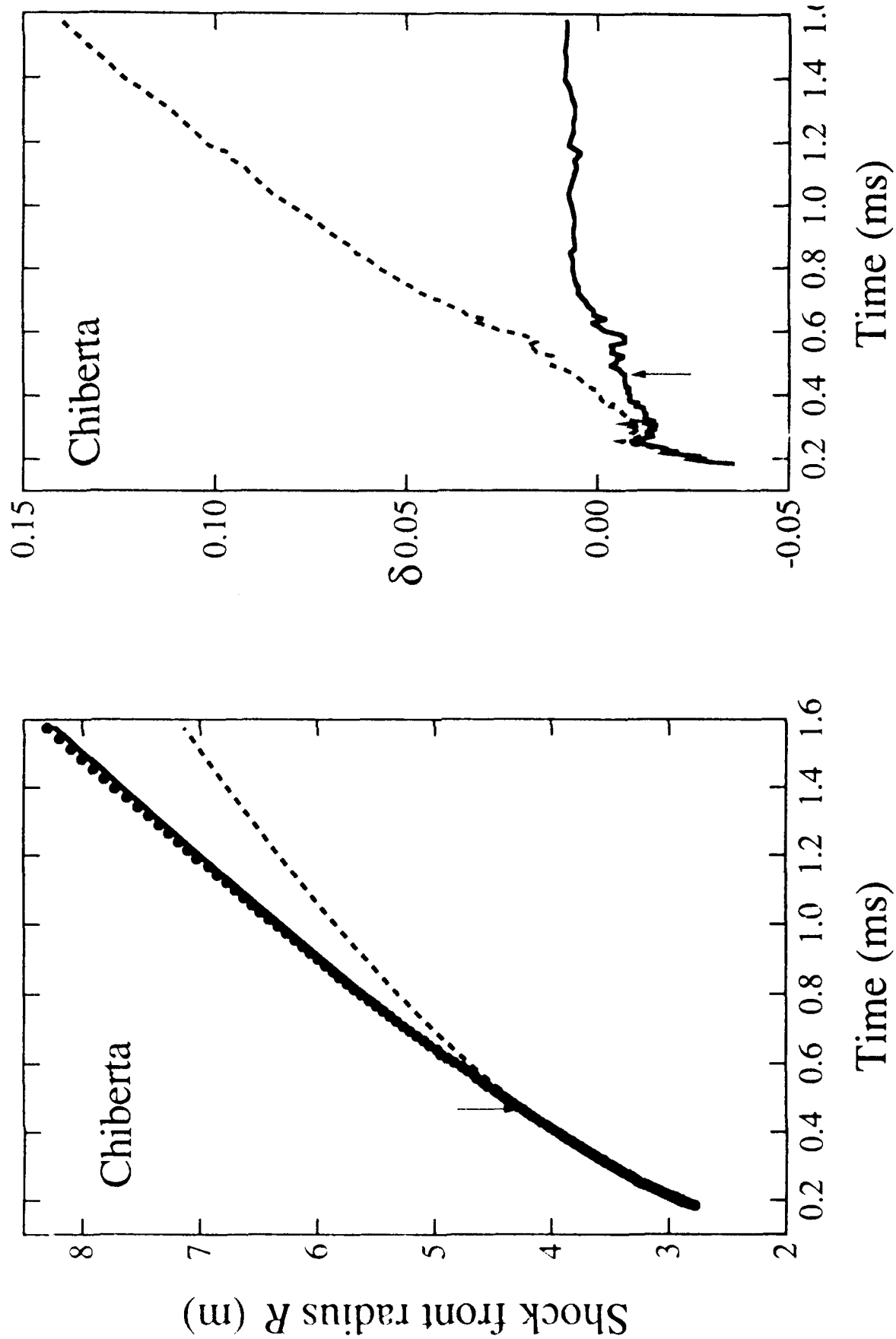
Fig. 12

Fig. 13

Fig. A1

Fig. A2

Fig. A3

Wet Tuff

Post-shock particle speed u_1 (km/s)

Shock front radius R (m)

Fig. A4

Fig. A5

SiO$_2$

Post-shock pressure p_1 (GPa)

Post-shock pressure p_1 (kbar)

Shock front radius R (m)
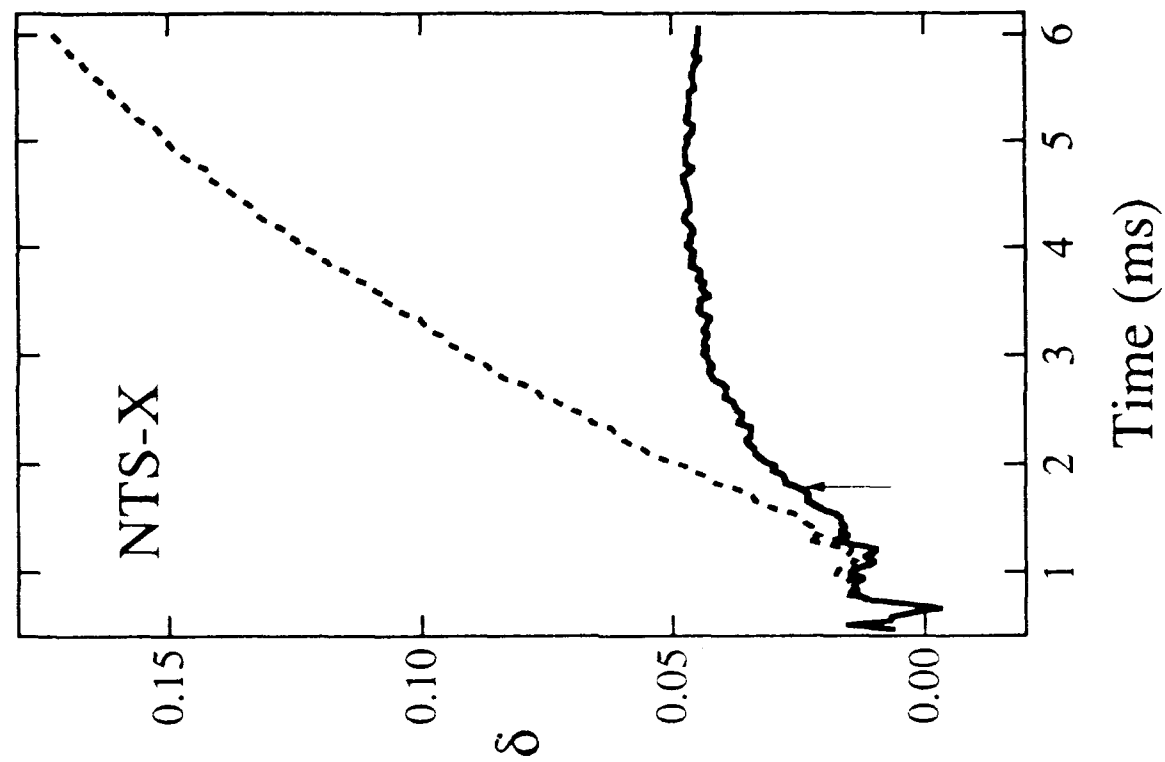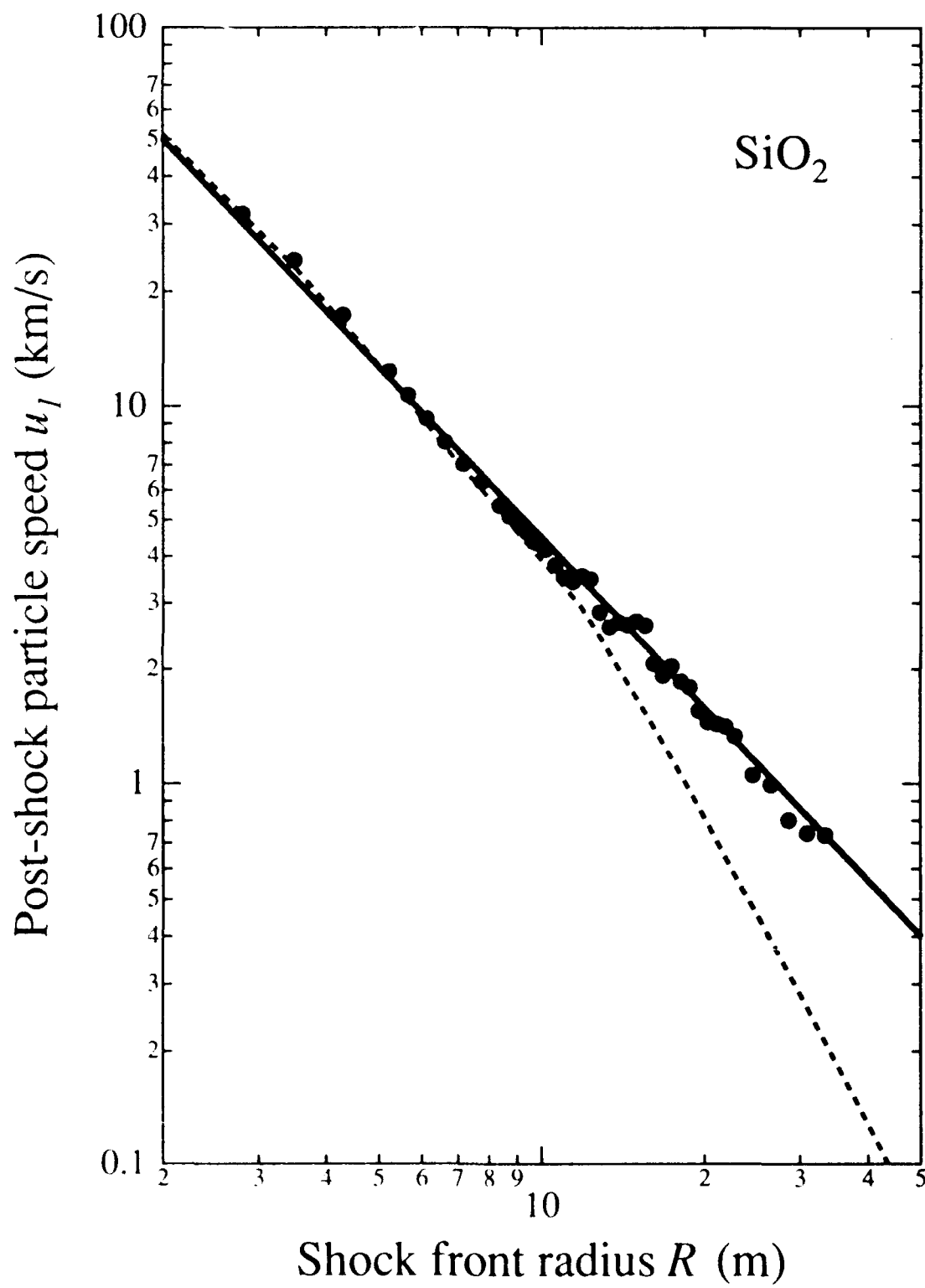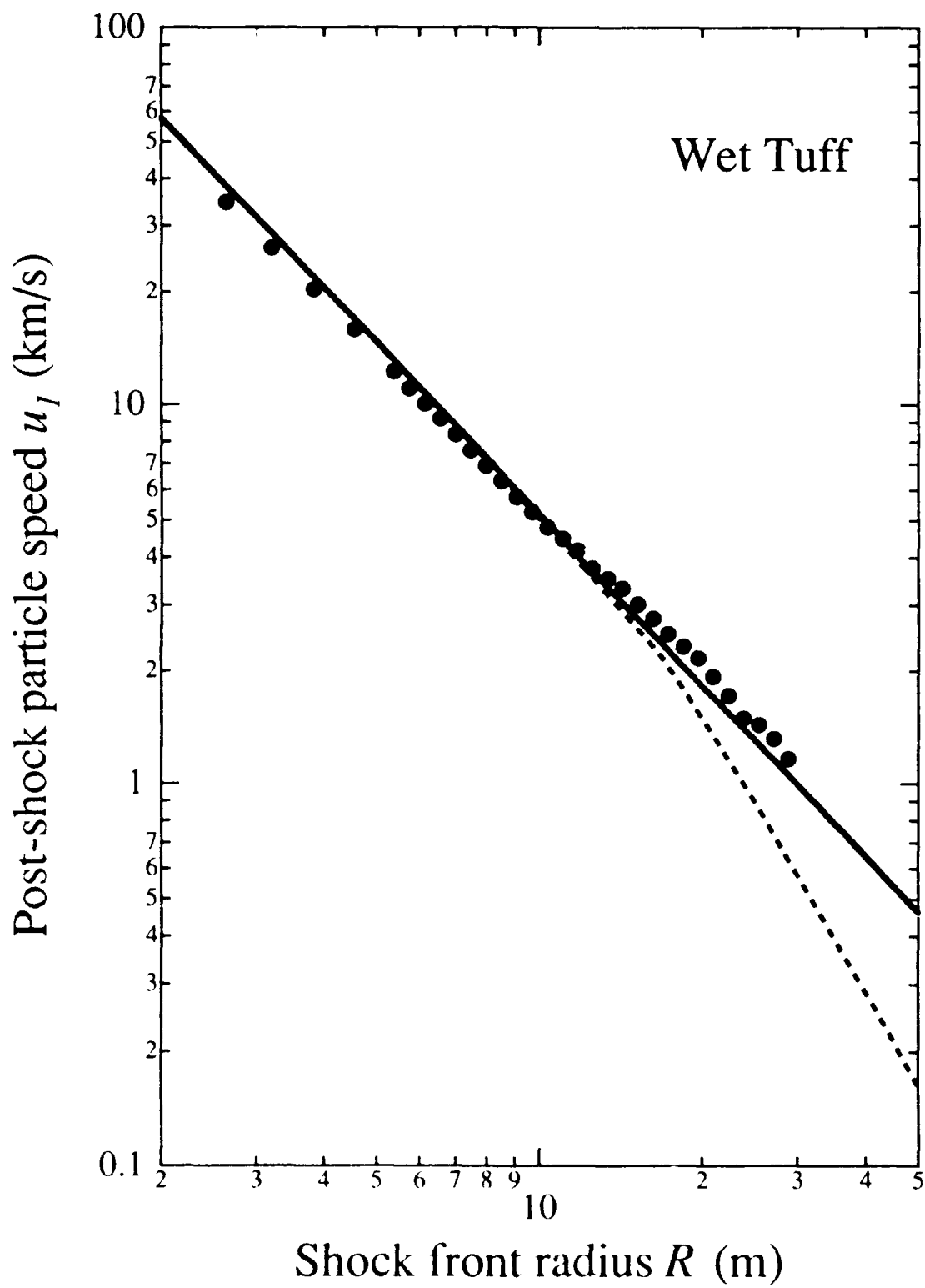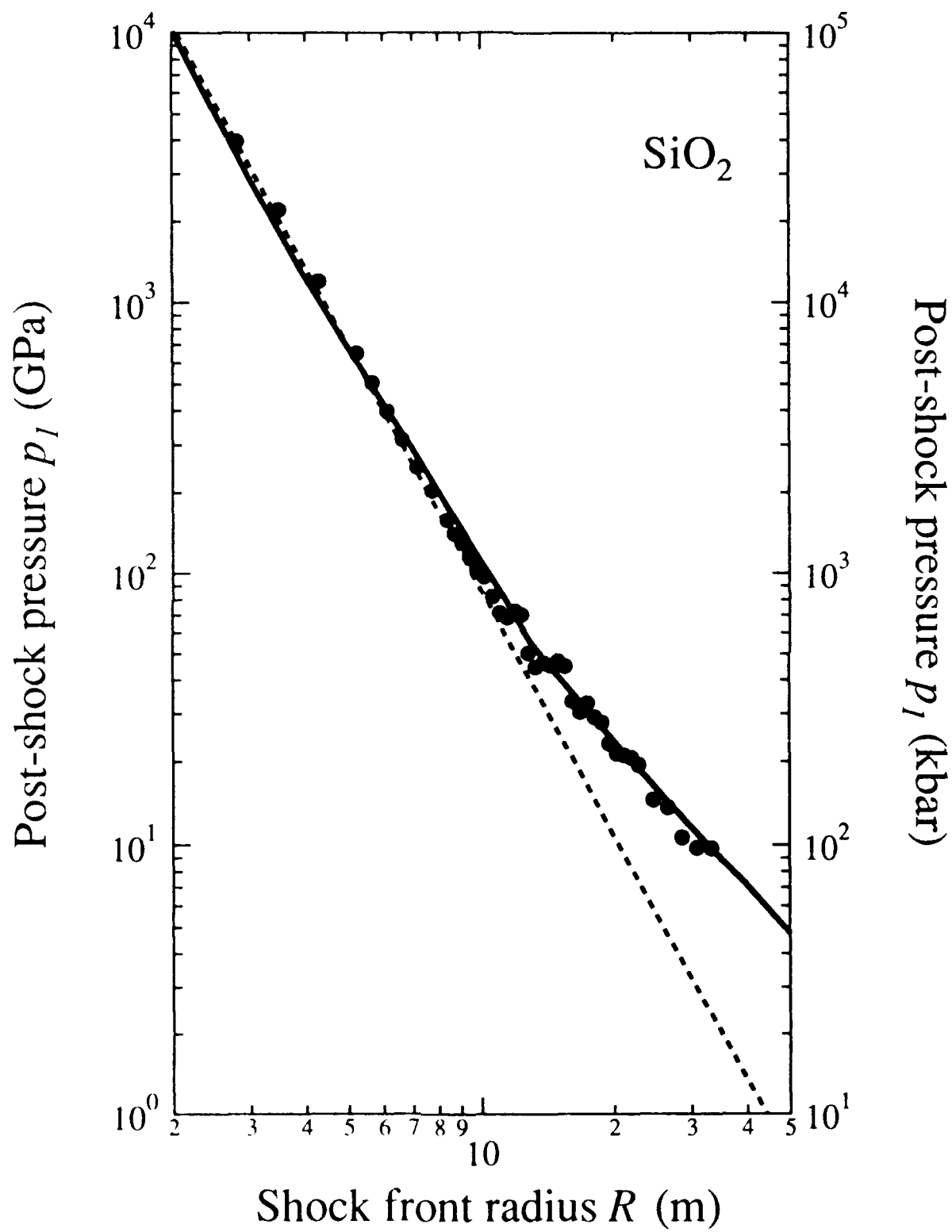
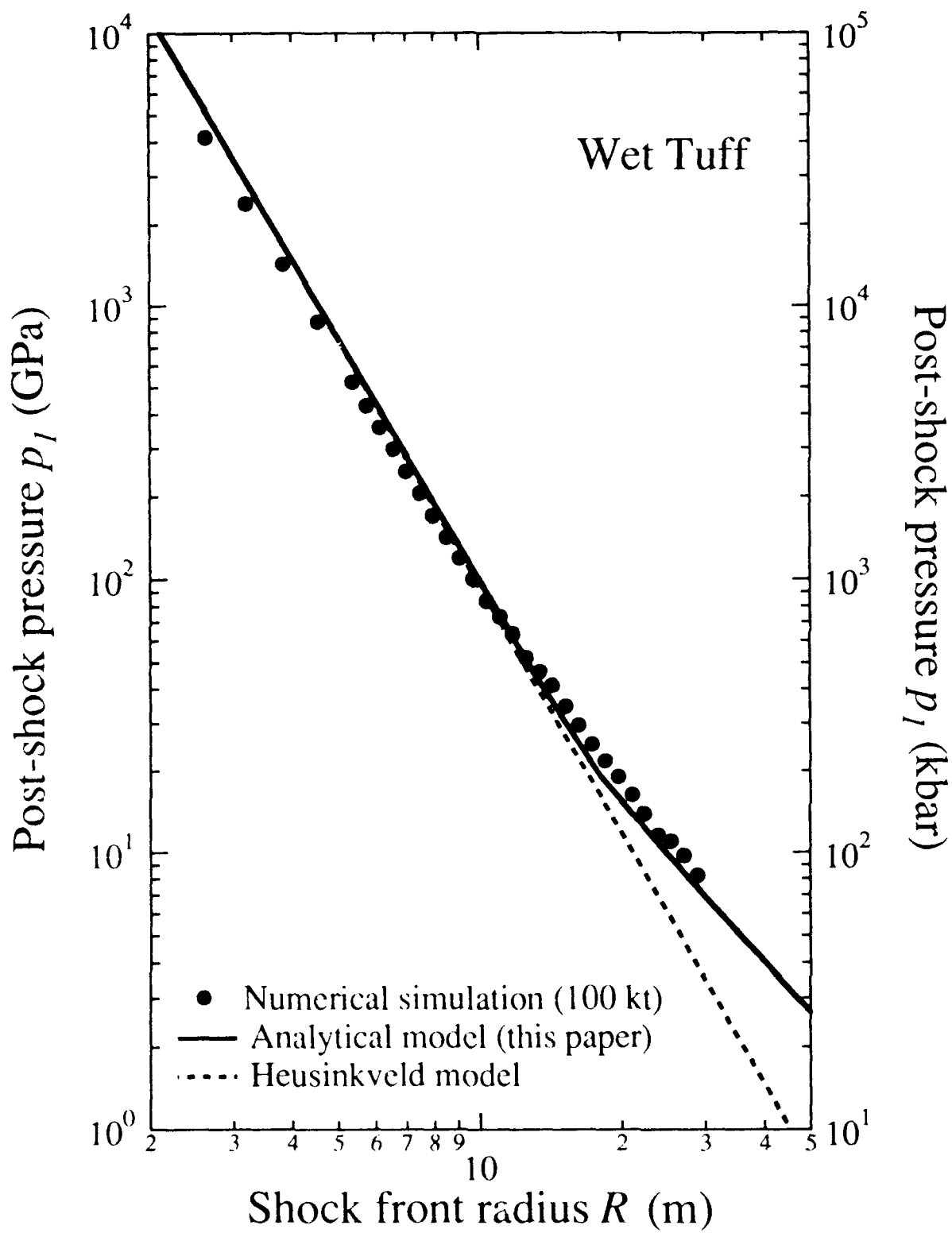Fig. A6

Prof. Thomas Ahrens
Seismological Lab, 252-21
Division of Geological & Planetary Sciences
California Institute of Technology
Pasadena, CA 91125

Prof. Keiiti Aki
Center for Earth Sciences
University of Southern California
University Park
Los Angeles, CA 90089-0741

Prof. Shelton Alexander
Geosciences Department
403 Deike Building
The Pennsylvania State University
University Park, PA 16802

Dr. Ralph Alewine, III
DARPA/NMRO
3701 North Fairfax Drive
Arlington, VA 22203-1714

Prof. Charles B. Archambeau
CIRES
University of Colorado
Boulder, CO 80309

Dr. Thomas C. Bache, Jr.
Science Applications Int'l Corp.
10260 Campus Point Drive
San Diego, CA 92121 (2 copies)

Prof. Muawia Barazangi
Institute for the Study of the Continent
Cornell University
Ithaca, NY 14853

Dr. Jeff Barker
Department of Geological Sciences
State University of New York
 at Binghamton
Vestal, NY 13901

Dr. Douglas R. Baumgardt
ENSCO, Inc
5400 Port Royal Road
Springfield, VA 22151-2388

Dr. Susan Beck
Department of Geosciences
Building #77
University of Arizona
Tuscon, AZ 85721

Dr. T.J. Bennett
S-CUBED
A Division of Maxwell Laboratories
11800 Sunrise Valley Drive, Suite 1212
Reston, VA 22091

Dr. Robert Blandford
AFTAC/TT, Center for Seismic Studies
1300 North 17th Street
Suite 1450
Arlington, VA 22209-2308

Dr. G.A. Bollinger
Department of Geological Sciences
Virginia Polytechnical Institute
21044 Derring Hall
Blacksburg, VA 24061

Dr. Stephen Bratt
Center for Seismic Studies
1300 North 17th Street
Suite 1450
Arlington, VA 22209-2308

Dr. Lawrence Burdick
Woodward-Clyde Consultants
566 El Dorado Street
Pasadena, CA 91109-3245

Dr. Robert Burridge
Schlumberger-Doll Research Center
Old Quarry Road
Ridgefield, CT 06877

Dr. Jerry Carter
Center for Seismic Studies
1300 North 17th Street
Suite 1450
Arlington, VA 22209-2308

Dr. Eric Chael
Division 9241
Sandia Laboratory
Albuquerque, NM 87185

Prof. Vernon F. Cormier
Department of Geology & Geophysics
U-45, Room 207
University of Connecticut
Storrs, CT 06268

Prof. Steven Day
Department of Geological Sciences
San Diego State University
San Diego, CA 92182

Marvin Denny
U.S. Department of Energy
Office of Arms Control
Washington, DC 20585

Dr. Zoltan Der
ENSCO, Inc.
5400 Port Royal Road
Springfield, VA 22151-2388

Prof. Adam Dziewonski
Hoffman Laboratory, Harvard University
Dept. of Earth Atmos. & Planetary Sciences
20 Oxford Street
Cambridge, MA 02138

Prof. John Ebel
Department of Geology & Geophysics
Boston College
Chestnut Hill, MA 02167

Eric Fielding
SNEE Hall
INSTOC
Cornell University
Ithaca, NY 14853

Dr. Mark D. Fisk
Mission Research Corporation
735 State Street
P.O. Drawer 719
Santa Barbara, CA 93102

Prof Stanley Flatte
Applied Sciences Building
University of California, Santa Cruz
Santa Cruz, CA 95064

Dr. John Foley
NER-Geo Sciences
1100 Crown Colony Drive
Quincy, MA 02169

Prof. Donald Forsyth
Department of Geological Sciences
Brown University
Providence, RI 02912

Dr. Art Frankel
U.S. Geological Survey
922 National Center
Reston, VA 22092

Dr. Cliff Frolich
Institute of Geophysics
8701 North Mopac
Austin, TX 78759

Dr. Holly Given
IGPP, A-025
Scripps Institute of Oceanography
University of California, San Diego
La Jolla, CA 92093

Dr. Jeffrey W. Given
SAIC
10260 Campus Point Drive
San Diego, CA 92121

Dr. Dale Glover
Defense Intelligence Agency
ATTN: ODT-1B
Washington, DC 20301

Dr. Indra Gupta
Teledyne Geotech
314 Montgomery Street
Alexanderia, VA 22314

Dan N. Hagedon
Pacific Northwest Laboratories
Battelle Boulevard
Richland, WA 99352

Dr. James Hannon
Lawrence Livermore National Laboratory
P.O. Box 808
L-205
Livermore, CA 94550

Dr. Roger Hansen
HQ AFTAC/TTR
Patrick AFB, FL 32925-6001

Prof. David G. Harkrider
Seismological Laboratory
Division of Geological & Planetary Sciences
California Institute of Technology
Pasadena, CA 91125

Prof. Danny Harvey
CIRES
University of Colorado
Boulder, CO 80309

Prof. Donald V. Helmberger
Seismological Laboratory
Division of Geological & Planetary Sciences
California Institute of Technology
Pasadena, CA 91125

Prof. Eugene Herrin
Institute for the Study of Earth and Man
Geophysical Laboratory
Southern Methodist University
Dallas, TX 75275

Prof. Robert B. Herrmann
Department of Earth & Atmospheric Sciences
St. Louis University
St. Louis, MO 63156

Prof. Lane R. Johnson
Seismographic Station
University of California
Berkeley, CA 94720

Prof. Thomas H. Jordan
Department of Earth, Atmospheric &
  Planetary Sciences
Massachusetts Institute of Technology
Cambridge, MA 02139

Prof. Alan Kafka
Department of Geology & Geophysics
Boston College
Chestnut Hill, MA 02167

Robert C. Kemerait
ENSCO, Inc.
445 Pineda Court
Melbourne, FL 32940

Dr. Max Koontz
U.S. Department of Energy/DP 5
Forrestal Building
1000 Independence Avenue
Washington, DC 20585

Dr. Fred LaCoss
MIT Lincoln Laboratory, M-200B
P.O. Box 73
Lexington, MA 02173-0073

Dr. Fred K. Lamb
University of Illinois at Urbana-Champaign
Department of Physics
1110 West Green Street
Urbana, IL 61801

Prof. Charles A. Langston
Geosciences Department
403 Deike Building
The Pennsylvania State University
University Park, PA 16802

Jim Lawson, Chief Geophysicist
Oklahoma Geological Survey
Oklahoma Geophysical Observatory
P.O. Box 8
Leonard, OK 74043-0008

Prof. Thorne Lay
Institute of Tectonics
Earth Science Board
University of California, Santa Cruz
Santa Cruz, CA 95064

Dr. William Leith
U.S. Geological Survey
Mail Stop 928
Reston, VA 22092

Mr. James F. Lewkowicz
Phillips Laboratory/GPEH
Hanscom AFB, MA 01731-5000(2 copies)

Mr. Alfred Lieberman
ACDA/VI-OA State Department Building
Room 5726
320-21st Street, NW
Washington, DC 20451

Prof. L. Timothy Long
School of Geophysical Sciences
Georgia Institute of Technology
Atlanta, GA 30332

Dr. Randolph Martin, III
New England Research, Inc.
76 Olcott Drive
White River Junction, VT 05001

Dr. Robert Masse
Denver Federal Building
Box 25046, Mail Stop 967
Denver, CO 80225

Dr. Gary McCartor
Department of Physics
Southern Methodist University
Dallas, TX 75275

Prof. Thomas V. McEvilly
Seismographic Station
University of California
Berkeley, CA 94720

Prof. John A. Orcutt
IGPP, A-025
Scripps Institute of Oceanography
University of California, San Diego
La Jolla, CA 92093

Dr. Art McGarr
U.S. Geological Survey
Mail Stop 977
U.S. Geological Survey
Menlo Park, CA 94025

Prof. Jeffrey Park
Kline Geology Laboratory
P.O. Box 6666
New Haven, CT 06511-8130

Dr. Keith L. McLaughlin
S-CUBED
A Division of Maxwell Laboratory
P.O. Box 1620
La Jolla, CA 92038-1620

Dr. Howard Patton
Lawrence Livermore National Laboratory
L-025
P.O. Box 808
Livermore, CA 94550

Stephen Miller & Dr. Alexander Florence
SRI International
333 Ravenswood Avenue
Box AF 116
Menlo Park, CA 94025-3493

Dr. Frank Pilotte
HQ AFTAC/TT
Patrick AFB, FL 32925-6001

Prof. Bernard Minster
IGPP, A-025
Scripps Institute of Oceanography
University of California, San Diego
La Jolla, CA 92093

Dr. Jay J. Pulli
Radix Systems, Inc.
2 Taft Court, Suite 203
Rockville, MD 20850

Prof. Brian J. Mitchell
Department of Earth & Atmospheric Sciences
St. Louis University
St. Louis, MO 63156

Dr. Robert Reinke
ATTN: FCTVTD
Field Command
Defense Nuclear Agency
Kirtland AFB, NM 87115

Mr. Jack Murphy
S-CUBED
A Division of Maxwell Laboratory
11800 Sunrise Valley Drive, Suite 1212
Reston, VA 22091 (2 Copies)

Prof. Paul G. Richards
Lamont-Doherty Geological Observatory
 of Columbia University
Palisades, NY 10964

Dr. Keith K. Nakanishi
Lawrence Livermore National Laboratory
L-025
P.O. Box 808
Livermore, CA 94550

Mr. Wilmer Rivers
Teledyne Geotech
314 Montgomery Street
Alexandria, VA 22314

Dr. Carl Newton
Los Alamos National Laboratory
P.O. Box 1663
Mail Stop C335, Group ESS-3
Los Alamos, NM 87545

Dr. George Rothe
HQ AFTAC/TTR
Patrick AFB, FL 32925-6001

Dr. Bao Nguyen
HQ AFTAC/TTR
Patrick AFB, FL 32925-6001

Dr. Alan S. Ryall, Jr.
DARPA/NMRO
3701 North Fairfax Drive
Arlington, VA 22209-1714

Dr. Richard Sailor
TASC, Inc.
55 Walkers Brook Drive
Reading, MA 01867

Prof. Charles G. Sammis
Center for Earth Sciences
University of Southern California
University Park
Los Angeles, CA 90089-0741

Prof. Christopher H. Scholz
Lamont-Doherty Geological Observatory
 of Columbia University
Palisades, CA 10964

Dr. Susan Schwartz
Institute of Tectonics
1156 High Street
Santa Cruz, CA 95064

Secretary of the Air Force
(SAFRD)
Washington, DC 20330

Office of the Secretary of Defense
DDR&E
Washington, DC 20330

Thomas J. Sereno, Jr.
Science Application Int'l Corp.
10260 Campus Point Drive
San Diego, CA 92121

Dr. Michael Shore
Defense Nuclear Agency/SPSS
6801 Telegraph Road
Alexandria, VA 22310

Dr. Matthew Sibol
Virginia Tech
Seismological Observatory
4044 Derring Hall
Blacksburg, VA 24061-0420

Prof. David G. Simpson
IRIS, Inc.
1616 North Fort Myer Drive
Suite 1440
Arlington, VA 22209

Donald L. Springer
Lawrence Livermore National Laboratory
L-025
P.O. Box 808
Livermore, CA 94550

Dr. Jeffrey Stevens
S-CUBED
A Division of Maxwell Laboratory
P.O. Box 1620
La Jolla, CA 92038-1620

Lt. Col. Jim Stobie
ATTN: AFOSR/NL
Bolling AFB
Washington, DC 20332-6448

Prof. Brian Stump
Institute for the Study of Earth & Man
Geophysical Laboratory
Southern Methodist University
Dallas, TX 75275

Prof. Jeremiah Sullivan
University of Illinois at Urbana-Champaign
Department of Physics
1110 West Green Street
Urbana, IL 61801

Prof. L. Sykes
Lamont-Doherty Geological Observatory
 of Columbia University
Palisades, NY 10964

Dr. David Taylor
ENSCO, Inc.
445 Pineda Court
Melbourne, FL 32940

Dr. Steven R. Taylor
Los Alamos National Laboratory
P.O. Box 1663
Mail Stop C335
Los Alamos, NM 87545

Prof. Clifford Thurber
University of Wisconsin-Madison
Department of Geology & Geophysics
1215 West Dayton Street
Madison, WS 53706

Prof. M. Nafi Toksoz
Earth Resources Lab
Massachusetts Institute of Technology
42 Carleton Street
Cambridge, MA 02142

5

Dr. Larry Turnbull
CIA-OSWR/NED
Washington, DC 20505

Dr. Gregory van der Vink
IRIS, Inc.
1616 North Fort Myer Drive
Suite 1440
Arlington, VA 22209

Dr. Karl Veith
EG&G
5211 Auth Road
Suite 240
Suitland, MD 20746

Prof. Terry C. Wallace
Department of Geosciences
Building #77
University of Arizona
Tuscon, AZ 85721

Dr. Thomas Weaver
Los Alamos National Laboratory
P.O. Box 1663
Mail Stop C335
Los Alamos, NM 87545

Dr. William Wortman
Mission Research Corporation
8560 Cinderbed Road
Suite 700
Newington, VA 22122

Prof. Francis T. Wu
Department of Geological Sciences
State University of New York
 at Binghamton
Vestal, NY 13901

AFTAC/CA
(STINFO)
Patrick AFB, FL 32925-6001

DARPA/PM
3701 North Fairfax Drive
Arlington, VA 22203-1714

DARPA/RMO/RETRIEVAL
3701 North Fairfax Drive
Arlington, VA 22203-1714

DARPA/RMO/SECURITY OFFICE
3701 North Fairfax Drive
Arlington, VA 22203-1714

HQ DNA
ATTN: Technical Library
Washington, DC 20305

Defense Intelligence Agency
Directorate for Scientific & Technical Intelligence
ATTN: DTIB
Washington, DC 20340-6158

Defense Technical Information Center
Cameron Station
Alexandria, VA 22314 (2 Copies)

TACTEC
Battelle Memorial Institute
505 King Avenue
Columbus, OH 43201 (Final Report)

Phillips Laboratory
ATTN: XPG
Hanscom AFB, MA 01731-5000

Phillips Laboratory
ATTN: GPE
Hanscom AFB, MA 01731-5000

Phillips Laboratory
ATTN: TSML
Hanscom AFB, MA 01731-5000

Dr. Michel Bouchon
I.R.I.G.M.-B.P. 68
38402 St. Martin D'Heres
Cedex, FRANCE

Dr. Michel Campillo
Observatoire de Grenoble
I.R.I.G.M.-B.P. 53
38041 Grenoble, FRANCE

Dr. Jorg Schlittenhardt
Federal Institute for Geosciences & Nat'l Res.
Postfach 510153
D-3000 Hannover 51, GERMANY

Dr. Kin Yip Chun
Geophysics Division
Physics Department
University of Toronto
Ontario, CANADA

Dr. Johannes Schweitzer
Institute of Geophysics
Ruhr University/Bochum
P.O. Box 1102148
4360 Bochum 1, GERMANY

Prof. Hans-Peter Harjes
Institute for Geophysic
Ruhr University/Bochum
P.O. Box 102148
4630 Bochum 1, GERMANY

Prof. Eystein Husebye
NTNF/NORSAR
P.O. Box 51
N-2007 Kjeller, NORWAY

David Jepsen
Acting Head, Nuclear Monitoring Section
Bureau of Mineral Resources
Geology and Geophysics
G.P.O. Box 378, Canberra, AUSTRALIA

Ms. Eva Johannisson
Senior Research Officer
National Defense Research Inst.
P.O. Box 27322
S-102 54 Stockholm, SWEDEN

Dr. Peter Marshall
Procurement Executive
Ministry of Defense
Blacknest, Brimpton
Reading FG7-FRS, UNITED KINGDOM

Dr. Bernard Massinon, Dr. Pierre Mechler
Societe Radiomana
27 rue Claude Bernard
75005 Paris, FRANCE (2 Copies)

Dr. Svein Mykkeltveit
NTNT/NORSAR
P.O. Box 51
N-2007 Kjeller, NORWAY (3 Copies)

Prof. Keith Priestley
University of Cambridge
Bullard Labs, Dept. of Earth Sciences
Madingley Rise, Madingley Road
Cambridge CB3 OEZ, ENGLAND